European Commission

JRC SCIENTIFIC AND POLICY REPORTS

Passive Automatic Identification System for Maritime Surveillance

Vladimir Kyovtorov; Michele Vespe; Joaquim Fortuny-Guasch; Dario Tarchi; Raimondo Giuliani; Joan Broussolle

2012

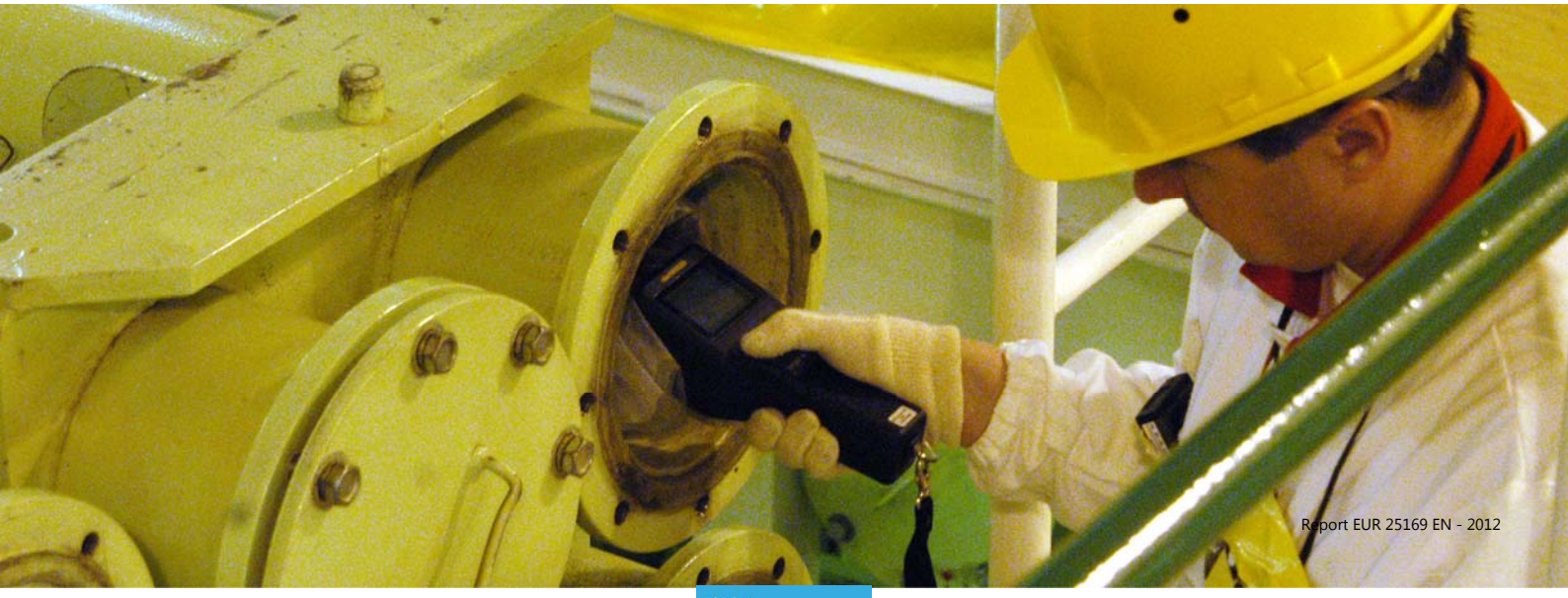

Report EUR 25169 EN - 2012

Joint Research Centre

European Commission
Joint Research Centre
Institute for the Protection and Security of the Citizen

Contact information
Ms. Alessandra Zampieri - Head of Unit
Address: Joint Research Centre, Via Enrico Fermi 2749, TP 670, 21027 Ispra (VA), Italy
E-mail: mare@jrc.ec.europa.eu
Tel.: +39 0332783894
Fax: +39 033278 9156

http://ipsc.jrc.ec.europa.eu/
http://www.jrc.ec.europa.eu/

JRC68405

EUR 25169 EN

ISBN 978-92-79-22730-1

ISSN 1831-9424

doi:10.2788/62028

Luxembourg: Publications Office of the European Union, 2012

Printed in Italy

C O N T E N T S

1. Introduction - The purpose of the work and objectives of the project

In compliance with the International Maritime Organization (IMO) regulation [34], ships (300 gross tonnage and upwards in international voyages, 500 and upwards for cargoes not in international waters and passenger vessels) are obliged to be fitted with Automatic Identification System (AIS) equipment. AIS will also be required for fishing vessels with a length of more than 15m and sailing in water under the jurisdiction of Member States of the European Union [40]. AIS is a broadcasting technology having considerable coverage (Very High Frequency VHF propagation) and accurate positioning performance, though Global Navigation Satellite System (GNSS). Nevertheless, the cooperative nature of AIS makes it vulnerable to false or missing declarations.

This project makes use of AIS in an entirely novel way, representing a low cost solution to augment the information that can be derived from the existing AIS infrastructure. This is achieved by analyzing indirect reflections of the broadcast AIS signals. **The objective of this study is a first test of feasibility**, providing an insight into uncertainties related to system sensitivity ("are the reflected signals strong enough to be detected?"), multipath and sea clutter influence. The main expected advantages of the use of Passive AIS approach are:

- low complexity of receiver design;
- no need for transmission licenses;
- silent operation;
- low power consumption.

Based on the main expected advantages, the possible future applications can be easily deployable system for continuous sea observation, cheap supporting system for maritime control and surveillance purposes, anti spoofing applications etc.

This research is based on the principles of the Passive Coherent Location (PCL) approach [15], which exploits the radiation of non cooperative transmitters (illuminators of opportunity) to detect and track targets by their scattered energy. The Passive-AIS (P-AIS) concept represents the combination of a self-reporting (AIS) and a non-cooperative target (PCL), based on the use of the widespread AIS emissions as illuminators of opportunity (fig.1).

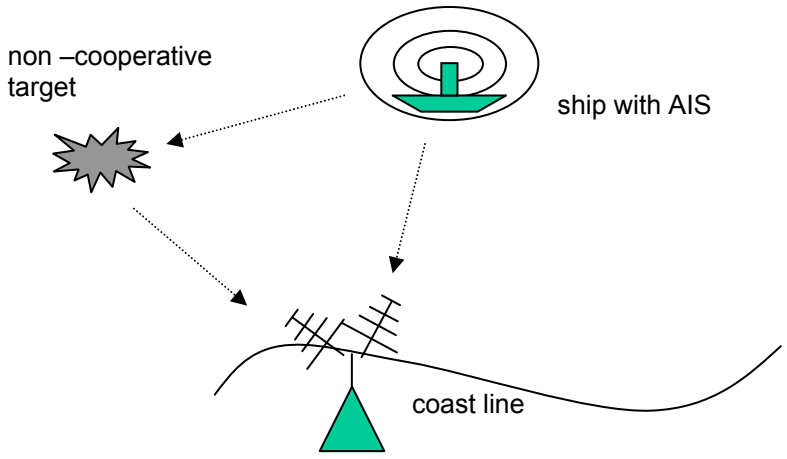

Figure 1: Passive AIS approach

As opposed to typical PCL applications that are characterised by a 3-D scenario, the maritime surveillance P-AIS is related to a 2-D one, which facilitates the unambiguous geo-location of the target. Like other VHF passive radar applications, P-AIS is characterised by (i) low frequency and low complexity of receiver design and (ii) larger Radar Cross Section (RCS) in comparison to C- and X-bands, which is due to resonance scattering, as the typical complex scatterers have a size comparable to the transmitted wavelength (~1.85 m) [41]. Furthermore, the specific added value of AIS as illuminator of opportunity resides in the possibility of implementing a time-separated multistatic network, where only one transmitter at a time is illuminating omnidirectionally in azimuth, preventing the overlapping in time of signals within the transmission channel [32].

This scientific report concerns the current obtained project results defining the performance limitations of a Passive AIS system. An extensive fundamental literature research has been made in order to find the peculiarities of the radio wave propagation and possible target reflection capabilities exactly within AIS frequency range and the clutter disturbance expectations. The resulted issues have formed the next task of experimental radio wave reflectivity determination of various maritime targets in different situations. Based on the obtained results a tool estimating the main energy expected in the receiver has been created. This tool has been used to outline the future passive radar system detection capabilities, based on the conventional Passive Coherent approach. The following results encourage conclusions and deliberations for further optimization of the passive AIS location approach.

The reminder of the work is organized as follows. Section 2 briefly presents the basic theoretical background on which the study is based. Section 3 describes the previous research that can be used in our objective. We subsequently define the main targets of further investigation and shape the relevant activities. Section 4 describes the results obtained and provides related discussion. Finally, Sections 5 presents final remarks and draws the future plans.

2. **Theoretical background**

2.1 Bistatic radars theory

Conventional passive radars are often arranged in bistatic configuration. The properties of bistatic radars are described in details in [14,34,40,7,4]. Classic bistatic geometry suitable for analysis and used in this work is shown in figure 2.

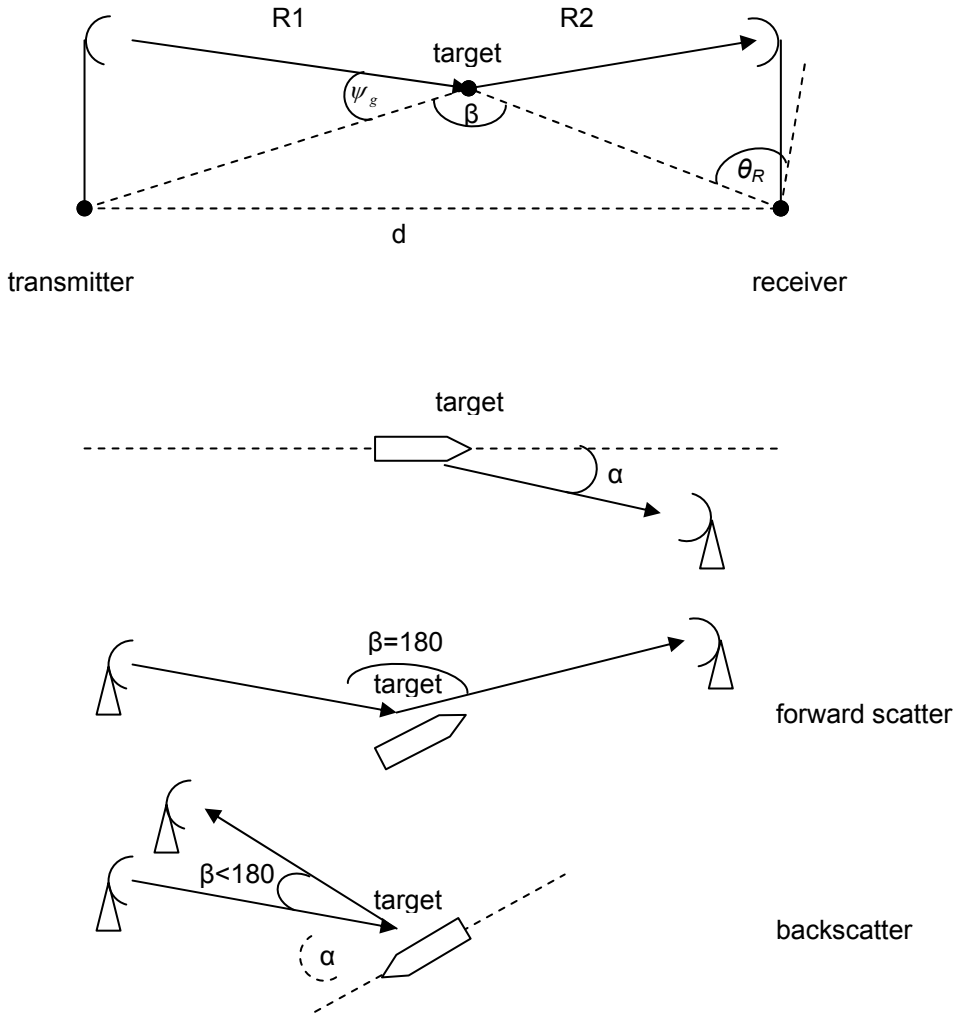

Figure 2: Bistatic radar geometry

where: *d* – is the base line, *R1* – target – transmitter distance; *R2* target - receiver distance, β – the bistatic angle (in some literature the bistatic angle is called aspect angle [3]); θ_R – azimuth towards the

target; ψ_g – grazing angle; α – aspect angle of target illumination. If β = 180*deg* a forward scattering mode appears, if $\beta < 180deg$ the mode is clearly backscattering. In order to understand whether the received signal is detectable in the presence of the inevitable noise, the basic and more important parameter Signal-to-Noise-Ratio (SNR) is introduced, which gives the strength of the signal against the noise power. The conventional bistatic radar equation is a well known expression giving the (SNR) at the receiving point [14, 40]:

$$SNR = \frac{\Pr}{Pn} = \frac{Pt\,Gt\,Gr\,\lambda^2\,\sigma_b\,F_t^2\,F_r^2\,G_p}{(4\pi)^3\,Rt^2\,Rr^2\,L\,k\,T_0\,B\,F} \tag{1}$$

where: *Pr* - the received power, *W*; *Pn* - the noise power, *W*; *SNR* - signal to noise ratio at the receiver; *Pt* – the transmitter power, *W*; *Gt* – the gain of the antenna transmitter, *ratio*; *Gr* – the gain of the antenna receiver, *ratio*; λ – the radar wavelength, *m*; *σb* – the bistatic Radar Cross Section, m^2; *Rt* – the distance between the transmitter and the target, *m*; *Rr* – the distance between the receiver and the target, *m*; k – the Boltzmann's constant, 1.38065*10^(-23); T_0 – noise reference temperature, 290 *K*; *B* – the receiver bandwidth, *Hz*; *F* - the receiver noise figure, *ratio*; *L* - the total loss from transmitter-target-receiver, *ratio*; *Ft* – pattern propagation factor transmitter-target, *ratio*; *Fr* - pattern propagation factor target-receiver, *ratio*; *Gp* – processing gain, *ratio*. This equation is the basic equation for initial scientific and engineering purposes. The factor $\frac{1}{Rt^2 Rr^2}$ has its maximum value for $Rt \to 0$ and $Rr \to 0$, hence the signal-to-noise value has its maximum, when the target is close either to the transmitter or the receiver. Because the signal processing is based on correlation, *Gp* measures the signal "augmentation" in the signal processing stage. It is described as:

$$G_p = t_{\max} * B \tag{1.a}$$

Basically, the longer the signal is the more "augmentation" has. For example if the bandwidth is *1.7MHz*, and pulse duration *1s*, the processing gain is *62.3dB* (from equation 1.a). On the other hand, if the pulse duration is *0.5s* the processing gain will be *59.3dB,* or *3dB* less "augmentation". In reality, the signal cannot be infinitively long and the processing gain is restricted by the maximum time allowing the processing gain - t_{max} - "time of the presence of the signal". It depends on the technical characteristics of the radar system and the "presence/mobility of the target". For example if the signal is long, but the target is fast, at certain time the target "escapes" from the position of interest. Therefore, t_{max} is subjected to the target acceleration:

$$t_{\max} = \left(\frac{\lambda}{A_R}\right)^{1/2} \tag{1.b}$$

where A_R is the value of the target acceleration [15]. The area having constant values of *SNR* is determined by the all possible $R_tR_r = const$ and has the well known oval of Cassini shape. As a difference, the conventional monostatic configuration has equidistant signal to noise concentric circumference areas [40].

2.2 Bistatic Radar Cross Section

Bistatic Radar Cross Section is a phenomenon still under investigation in the radar community [14,40,41]. By definition the radar cross section (RCS) is a measure of the "effective strength of a radar target reflection" [6]. This is the parameter describing the most important characteristic of any radar target and measures the ability to reflect the illuminated energy towards the radar receiving antenna. Generally its mathematical description is [6]:

$$\sigma = 4\pi \frac{Ps}{Pi} \tag{2}$$

Ps - is the power per unit solid angle scattered in a specific direction and *Pi* – is the power per unit area in a plane wave incident on the scatterer from a specific direction [6]. RCS of complex targets depends mainly on the target shape, coating, illuminating wavelength, polarisation and aspect angle. Considering the angle of illumination, three major cases are distinguished [6]: (1) *monostatic* or *backscattering* RCS when the incident or pertinent scattering directions are coincident, but opposite in

sense; (2) *forward scattering* RCS when the two directions and senses are the same; (3) *bistatic* RCS when the two directions are different (fig.2). The bistatic RCS also depends on the bistatic angle, turning the prediction of such parameter into a task of challenge.

Nevertheless, most literature sources compare the bistatic RCS with the monostatic and for analysis simplification assume that both RCS of complex object are similar for bistatic angles less than 90 deg [7, 40, 41]. Furthermore, the bistatic RCS might be higher than the monostatic RCS [4]. This phenomenon increases the possibility of using the bistatic radars approach in order to increase the SNR at the receiver.

2.3 Pattern propagation factor

The environment in which the radar operates can have considerable effect on the radar wave propagation. The nature of propagation is important because it affects both the radar coverage and the accuracy of measurements [33]. The free space radar performance is modified by (1) *reflections* from the surface of the earth, (2) *refraction* caused by an inhomogeneous atmosphere and (3) *attenuation* by the gases constituting the atmosphere. The reflection plays major role in the line of sight. The diffraction is "active" beyond the line of sight or over the horizon, whereas the attenuation strongly depends on the meteorological atmospheric conditions (precipitation, humidity, hails etc.). In general the theoretical analysis of the propagation does not usually give quantitative analysis for a precise radar design, because it depends on the environment in which the radar works. Therefore, no theoretical analysis could be done and the radar designers should have knowledge of the "average" propagation conditions. The reflection from the surface is ***smooth*** and ***rough***. The smooth reflection (specular reflection) is a coherent reflection of the radio wave from a smooth surface. Here the laws of optics are usually applied stating that the angle of reflection is equal to the angle of incidence. On the other hand, the reflection from rough surface causes diffuse reflection. In that case the total field at the target is sum of the direct ray, the specular component and the diffuse component. In the reflection process the angle of the wave incidence is called – grazing angle (fig.3 ψ_g). A critical grazing angle is defined by Rayleigh as the angle below which a surface is considered to be smooth, and above which a surface is considered to be rough [28,34,6,7,33]. Considering figure 3, denote the root mean square (rms) of a surface height irregularity as h_{rms}, then according to the Rayleigh criteria the surface is considered to be smooth if [28,6]:

$$\frac{4\pi h_{rms}}{\lambda}\sin\psi_g < \frac{\pi}{2} \tag{3}$$

where ψ_g it he grazing angle. The path between "smooth path" and the "rough path" is different by $2h_{rms}\sin\psi_g$, this path translates into phase difference:

$$\Delta\psi = \frac{2\pi}{\lambda}2h_{rms}\sin\psi_g \tag{4}$$

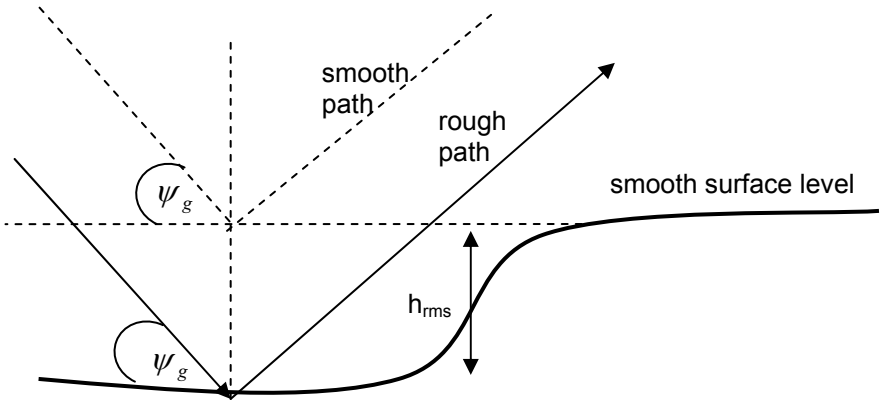

Figure 3: Rough surface definition [28]

The critical grazing angle now is

$$\psi_{gc} = \arcsin\frac{\lambda}{4h_{rms}} \tag{5}$$

In the maritime scenario h_{rms} is related to the height of the water wave, which depends on the sea state that is usually measured by the Beaufort scale [20]. The geometry for surface reflection of a simplified smooth surface is shown on the figure 4. From this geometry the following equations are easily derived [7]:

Target elevation	$\theta_t \approx (h_t - h_r)/R$	(6.1)
Grazing angle	$\psi_g \approx (h_t + h_r)/R$	(6.2)
Path length difference	$\delta_0 \approx 2h_t h_r / R$	(6.3)
Range to reflection point	$x_0 \approx Rh_r/(h_t + h_r)$	(6.4)

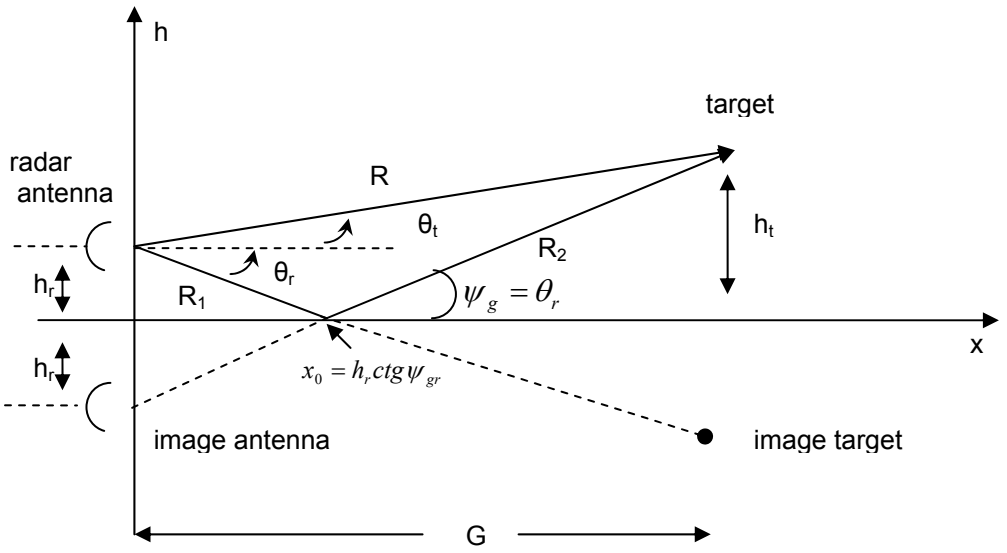

Figure 4: Geometry of specular reflection from a smooth (flat) surface [7]

Because P-AIS scenario implies ground base antenna positioning, the influences of the ambient environment, effects as reflection from the ground, reflection from surrounding objects, shadowing diffraction, multipath etc. play vital role in the detection process [6,33]. We assume that the reflection from the ground is one of the most important effects that could be considered. The geometry in Figure 4 is one of the most used scenario – the "two way propagation model", which reasonably approximates ground based line of sight surveillance systems [34, 6, 33]. The pattern propagation factor on the presence of surface reflection may be defined as a sum between the direct and reflected ray [5]:

$$F = \left| f(\theta_t) + f(-\psi_g)\rho D \exp(-ja) \right| \tag{7}$$

where $f(\theta)$ represents the direct ray; $f(-\psi_g)\rho D \exp(-ja)$ - is responsible for the reflected ray and includes the influence of the phase difference and the earth curvature; This formulation for F applies only for certain limit of path difference (when $\delta_0 > \lambda/6$). For smaller path differences, the effects of diffraction are dominant [7]. The effect of superposition between direct and reflected rays constructively and destructively alternates the received power – peaks and nulls appear. In fact those alternations are function of the target range as figure 5 shows. The dotted line is the free space return situation - no interference between direct and reflected rays.

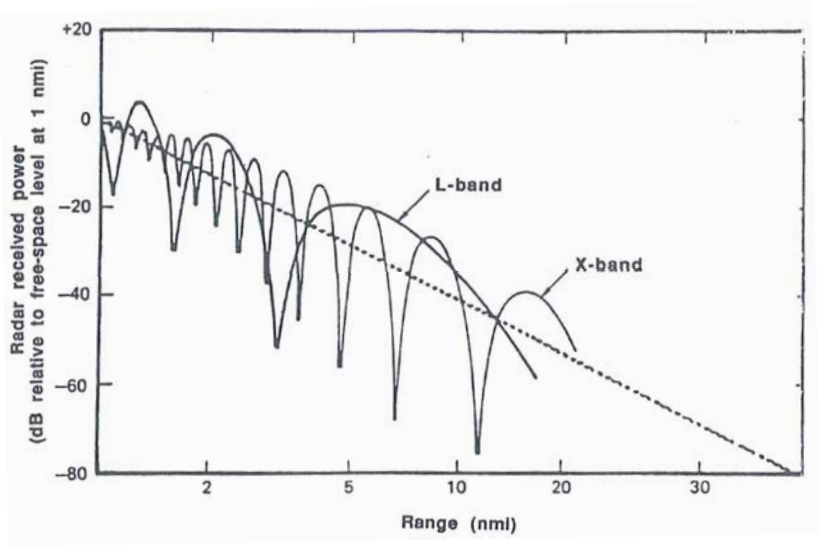

Figure 5: Pattern propagation factor [27]

Both peaks and nulls vary around the free space return but follow the free space on the average. For fixed conditions, the lowest interference lobe moves closer to the surface (further out in range) as the wavelength becomes shorter [27]. Therefore, in the case of VHF, which is the AIS frequency band, we more distinguishable zeros and nulls than the L-band curve on figure 5 are expected. Thus, the effective radiation (similarly to the receiving one for separate receiving antennas) pattern is changed into lobbing structure as figure 6 indicates. A target located at the maximum of a particular lobe is located at twice range distance as a comparison to the same radar located at free space. However, at other angles the radar detection range can be reduced with respect to that in free space. In some geometry, when the returns from multiple paths are in destructive interference, the target can be even transparent.

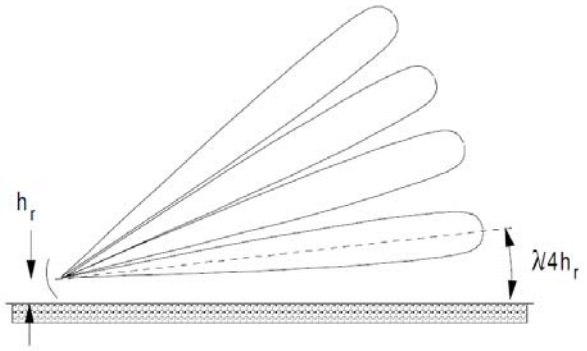

Figure 6: Multilobbed structure caused by surface reflection [6]

2.4 Effective RCS

In the practice usually the term "effective RCS" is used for RCS of point target modified by the pattern propagation factor F^4 ($F^2_t F^2_r$ in the bistatic case). The *RCSeff* (effective RCS) is defined as [6, 27, 10]:

$$\sigma_{eff} = \sigma F^4 \tag{8.1}$$

or in case of separated transmitting and receiving antennas:

$$\sigma_{eff} = \sigma_b Ft^2 Fr^2 \tag{8.2}$$

where σ_b is the bistatic target cross section. When measured in real environment, the *RCSeff* is already modulated by the pattern propagation factor, which does not need to be calculated separately to estimate the radar equation.

2.5. Theoretical description of sea Clutter

The clutter is defined as the undesired radar echo, typically coming form ground, sea, rain, birds, insects, aurora etc. [6]. There is no single definition because clutter might also be a target. For example, for the airborne radar the rain is clutter, but target for the weather radar. The effect of the clutter creates serious obstacles for real target detection and evaluation. Theoretically, the clutter has many sources of origin and consequently diverse statistics. Clutter can be classified into two main categories: surface (trees, vegetation, ground terrain, man-made structures, sea surface and volume (chaff, rain, birds, and insects) [28,34,6].

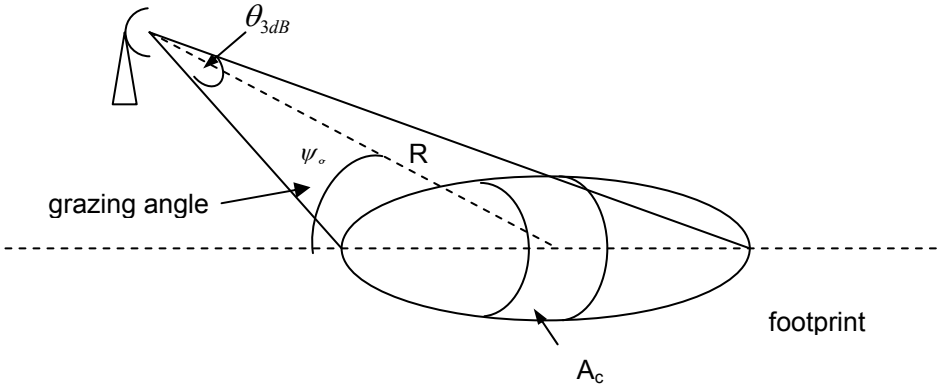

Figure 7: Geometry of the clutter

Clutter echo is often modelled as a random process and described by specific probability distributions. Sometimes it has bigger energy than the white noise. Then, the term Signal-to-Clutter Ratio (SCR) describing the ratio of reflected radio energy between the target and clutter, is used. The clutter backscatter can be determined as the equivalent radar cross section attributed to the reflections from a clutter area *Ac*:

$$\sigma_c = \sigma^0 Ac \tag{9}$$

where σ^0 is the normalized clutter RCS (clutter scattering coefficient), *Ac* the clutter area, defined by the radar range resolution. Our further studies consider the geometrical clutter scenario shown in fig. 7. The receiving antenna for P-AIS is directive and has small sidelobes level. Hence, the influence of the sidelobes on the clutter level can be neglected. In that case the area *Ac* is determined as:

$$A_c \approx R\theta_{3dB}\frac{c\tau}{2}\sec\psi_g \text{, where } \tau = \frac{1}{B},\ \sec\psi_g = \frac{1}{\cos\psi_g},\quad A_c \approx R\theta_{3dB}\frac{c}{2B\cos\psi_g} \tag{10}$$

For simplicity, let's take the basic radar equation for monostatic configuration. The signal returned in the radar could be described as:

$$St = \frac{PtG^2\lambda^2\sigma_t}{(4\pi)^3 R^4} \tag{11}$$

where, as usual, *Pt* – transmitter power, *G*-antenna gain; λ – length of the radio wave; σ_t - RCS of the target; *R* – distance to the target. Similarly the power retuned from the clutter can be described as:

$$Sc = \frac{PtG^2\lambda^2\sigma_c}{(4\pi)^3 R^4} \tag{12}$$

The Signal-to-Noise Ratio is:

$$SNR = \frac{Pt\,G^2\,\lambda^2\,\sigma_t}{(4\pi)^3 R^4 k T_0 B F L} \tag{13}$$

where *k*-Boltzman's constant, T_0- the effective noise temperature; *B* - radar operating bandwidth; *F*-receiver noise figure; *L*-total radar losses; Dividing eq. 12 by eq.11 we obtain Signal-to-Clutter-Ratio (SCR) [6]:

$$SCR = \frac{\sigma_t}{\sigma_c} = \frac{\sigma_t}{\sigma^0 Ac} \tag{14}$$

When the clutter statistics is Gaussian, the clutter signal return and the noise return can be combined and a new value for determining the radar measurement accuracy is derived from the Signal-to-Clutter-to-Noise Ratio or shortly Signal-to-Interference Ratio (SIR) [6]:

$$SIR = \frac{1}{\frac{1}{SNR} + \frac{1}{SCR}} \tag{15}$$

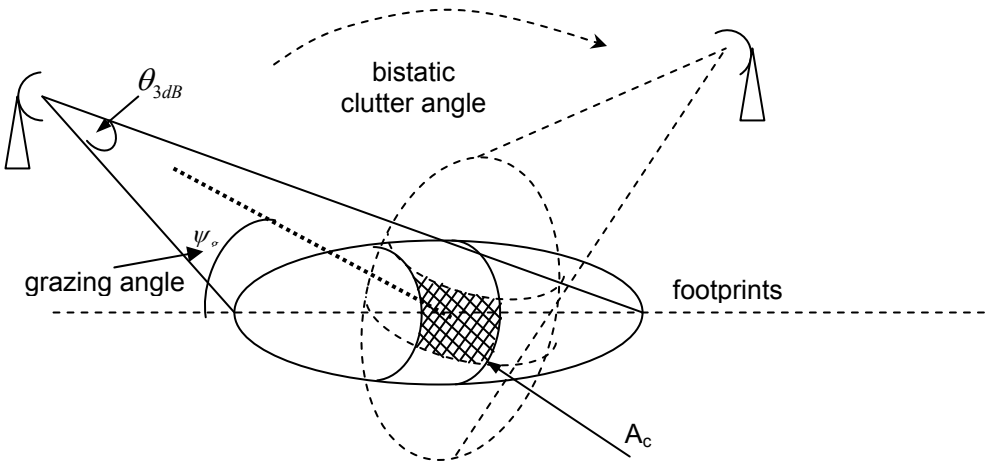

Figure 8: Geometry of the bistatic clutter

When the transmitting and receiving antennas are not colocated, the clutter contribution is "bistatic". The bistatic clutter is described as the monostatic in eq.9, where $\sigma^0 = \sigma_b^0$, i.e. the bistatic normalized clutter RCS (bistatic clutter scattering coefficient), and *Ac* is the area defined by the bistatic radar range resolution (the intersection of both transmitter and receiver antenna beams) fig. 8. The fact that the bistatic RCS depends additionally on the bistatic (horizontal) and the grazing (vertical) angle makes the bistatic clutter more complicated, hardly predictable and a topic of current investigations [3].

2.6 AIS outlines

AIS transponders automatically transmit various vessel parameters (position, time, velocity, course, type of ship etc.). This information is transmitted on time intervals. Except reporting their parameter to the maritime control centres via terrestrial or satellite network, the ships can communicate amongst each other. Wholely, the structure of the communication is complex and based on the self organization principles. The received information can be displayed on screen, plotted or forwarded further to specific users. The receivers are not standardized because they do not transmit. The AIS standard for transmitters comprises several sub standards, which specify the product type, integrity and the technical capabilities of the transponder. There are 27 different types of messages defined in the standard [19]. The transmission is specifically design in the VHF radio range. The AIS waveform is Gaussian Minimum Shift Keying (GMSK) modulated. For transmission, the original 9.6 kbps binary data stream is filtered through a Gaussian Low Pass Filter (LPF), obtaining a time-bandwidth product *BT* = 0.5. The pre-filtered signal is then frequency modulated over two channels 161.975 MHz or 162.025 MHz. For each channel, 2250 time slots are allocated within 60 seconds, according to the autonomously synchronized Time Division Multiple Access (TDMA) access scheme (i.e. Self-

Organising, Incremental and Random Access TDMA) [32]. As a result, the access scheme offers synchronised network of transmitters, without need for interrogation. The signal can be transmitted in 'low' or 'high' power setting, depending on the AIS traffic conditions: in port proximity, for instance, less power is required in order to avoid messages congestion, [32].

3. Background Description and Problem Formulation

Considering our main objective to explore the technical possibilities of using the AIS transponders as an illuminator of opportunity for passive ship surveillance, we might take into consideration at least the bistatic geometrical approach. In order to define the potential of such a system and to calculate its basic coverage we start from the bistatic radar equation (eq. 1) and take into consideration all the features of the parameters in the equation and the previous scientific experience in this field. The AIS polarization is strongly vertical [32], therefore we will not consider the cross-polarization peculiarities of the target and clutter properties.

In this work, the main analysed parameters for P-AIS detection capabilities are:

- Target bistatic RCS;
- Clutter bistatic backscatter;
- Pattern propagation factor effects for the specific frequency; the bandwidth and sea state.

The extensive literature survey showed that VHF bistatic radars for marine purposes are not entirely examined. On the other hand, this frequency range has some advantages like the propagation of the radio waves, which may enable to detect low-RCS targets and to increase the detection range [6, 9].

3.1 Bistatic RCS for P-AIS

Simple shape objects (spheres, cylinders, cones etc.) have increased theoretically estimated RCS as a function of the bistatic angle of illumination [40, 4]. Furthermore, as soon as the bistatic angle reaches 180*deg* a forward scattering phenomenon occurs, which consists of a significant RCS increase. Due to the nature of the scatters the bistatic RCS of a target strongly depends on the frequency. Little work has been carried out at VHF. Work [40] mentions a VHF bistatic RCS lower than the monostatic, except close to the forward scattering region. In [36, 35] a bistatic model, using monopoles for frequencies 8-12 MHz reveals that the bistatic RCS depends on the bistatic angle and could be higher or lower than the monostatic one. The work [15] also gives us some preliminary picture, about how the bistatic target RCS, having physical area 10 sq. meters, looks within VHF frequency of interests for forward scattering mode (fig.9). Here $\theta_b=\lambda/d$ represents the antenna beam width. For example, the $10m^2$ target area in forward scattered mode for 100MHz has RCS about 40 dBsm.

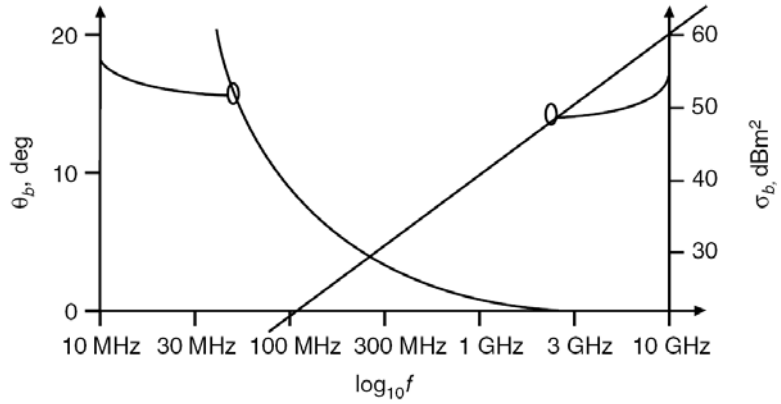

Figure 9: Variation of RCS σ_b and angular width θ_b of forward scatter of a target of physical area $10m^2$ and linear dimension 20m, against frequency [15]

A generalization for the difference between bistatic and monostatic RCS for 250MHz could be found in [41]: "most bistatic data are within ±3dB of the monostatic values, with and occasional excursion to

±6dB, for the $\beta=135^0$ (fig.10). Excluding the monostatic and bistatic specular peaks, this aspect-independent, nearly constant RCS phenomenon is typical of a target response in its resonance region" [13]. Considering the assumed bistatic scenario (fig. 2) the "aspect-independence" means independence of the bistatic angle. Another valuable work, worth to be mentioned, is a measurement of the RCS of large vessels in [12] (fig.11). Although this is not a study of bistatic target cross-section, the radar frequency is in VHF range.

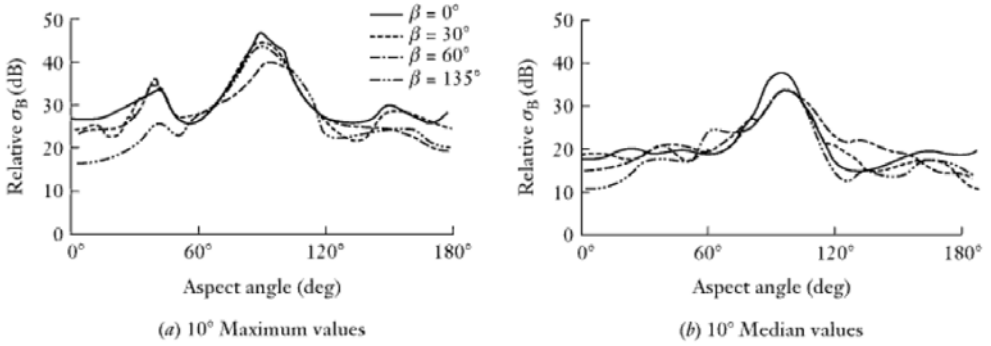

Figure 10: Relative monostatic and bistatic RCS for a B-47 jet aircraft at 250MHz, horizontal polarization [40,41]

This works gives real results for the effective monostatic RCS of a cargo ship between 25-50dBsm. Taking into consideration the comparisons between bistatic and monostatic RCS, cited above, this work could derive approximate expectations about the bistatic RCS in the range of AIS wavelength.

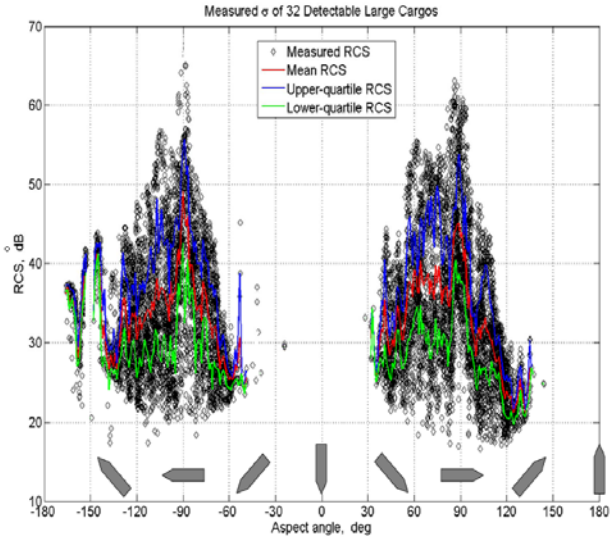

Figure 11: RCS value of 32 detectable large cargoes vs.ship aspect angle [12]

Summarizing the aforementioned in this paragraph and the extensive research amongst the literature, we can conclude, that

- The expected effective RCS value of medium maritime targets is about 20dBsm or higher depending on its size and shape.
- Wholely, there is no enough information about the bistatic RCS behaviour in the VHF frequency range. Then one of next goals is the derivation of some in-situ results and their use in the bistatic radar equation (1). Once the bistatic radar equation is validated, it can be used for any further applications in this frequency range.
- The differences between the monostatic and bistatic RCS, in VHF range, are about ±3dB.

3.2 Bistatic Clutter for P-AIS

The clutter in bistatic mode in the AIS frequency range (VHF) is also a subject of particular interest. Considering the range resolution cell or the bandwidth of the AIS signals, its contribution for the returned signal-to-noise ratio in the radar equation could be severe. For example, in low resolution application, when the cell size is in the order of kilometres, will give very large antenna footprint areas. Multiplication of the normalized clutter RCS by this area (eq.9) reveals a very strong influence of the clutter on the returned signal-to-noise ratio and the successive target detection probability. Although there is no clarity about what causes the bistatic clutter and what its major dependencies are, the literature survey gives good and helpful practical results for the monostatic clutter exactly in AIS frequency area of interest. The approximate differences between the monostatic and bistatic clutter values are concluded here [41].

The clutter reflection from the sea could be divided into several sub zones: near grazing incidence, plateau region; near vertical incidence [27]. Figure 12 shows the behaviour of the normalized clutter RCS (σ^0) as a function of the grazing angle. The boundaries of those zones depend on the wavelength, surface condition and polarization. In the near grazing incidence region normalized clutter RCS increases rapidly when the in grazing angle increases or the wavelength decreases. For the plateau region σ^0 changes slowly with grazing angle and transmitted wavelength; σ^0 for horizontal polarization is more sensitive on the wavelength than vertical polarization [27]. For small grazing angles and plateau region, the magnitude of σ^0 increases if the surface roughness increases. For vertical incidence, σ^0 tends to decrease in surface roughness increase and the dependence on the wavelength is less sensitive [27].

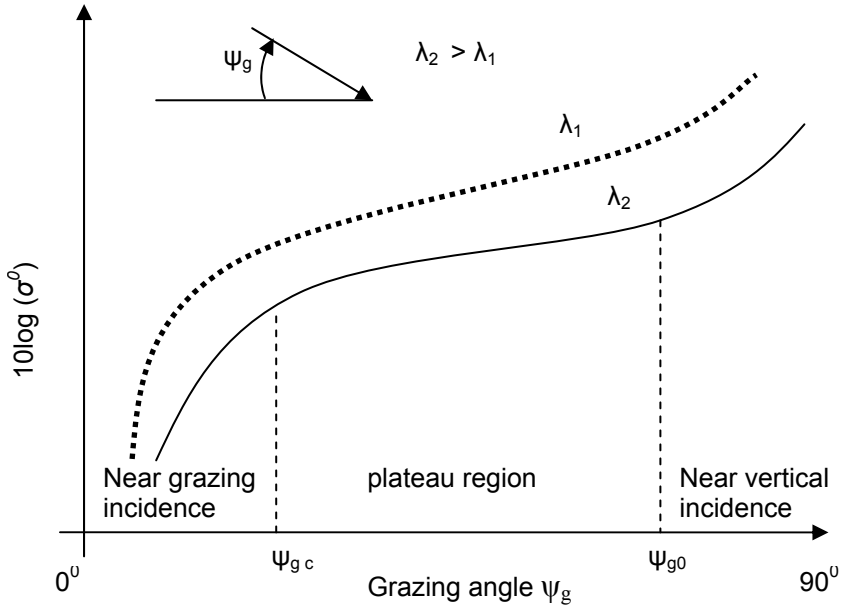

Figure 12: General dependence of σ^0 on grazing angle θ [27]

The vast majority of the literature normally reports valuable monostatic, and bistatic clutter behaviour results for the microwave frequency band (above L band) [40, 41, 39, 27]. The following question is posed: "What the typical bistatic clutter values as a function of grazing angle within VHF range are?" A recent publication about a test of low cost HF radar for surveillance of the Exclusive Economic Zone concerns mainly about the sea clutter [29]. It successfully simulates and measure the surface wave propagation loss and match these results to the Barrick relations [5].

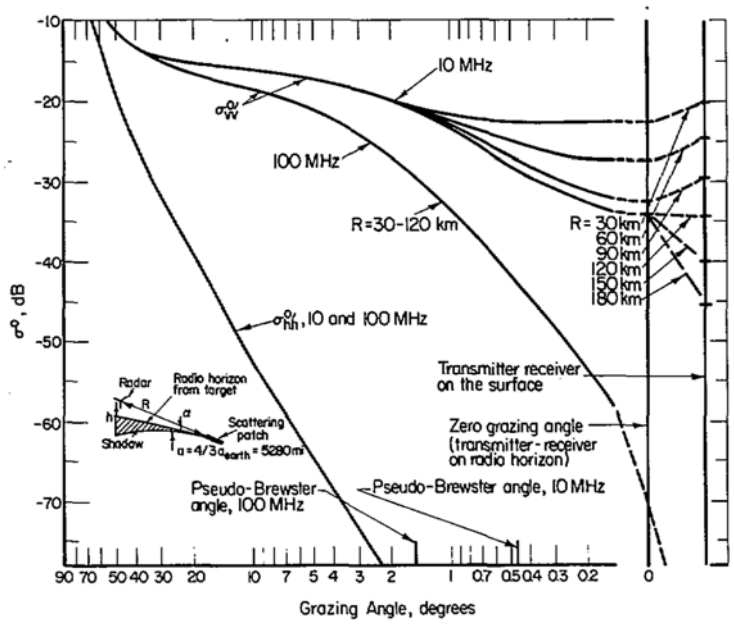

Figure 13: Dependence of received backscatter power on grazing angle [5]

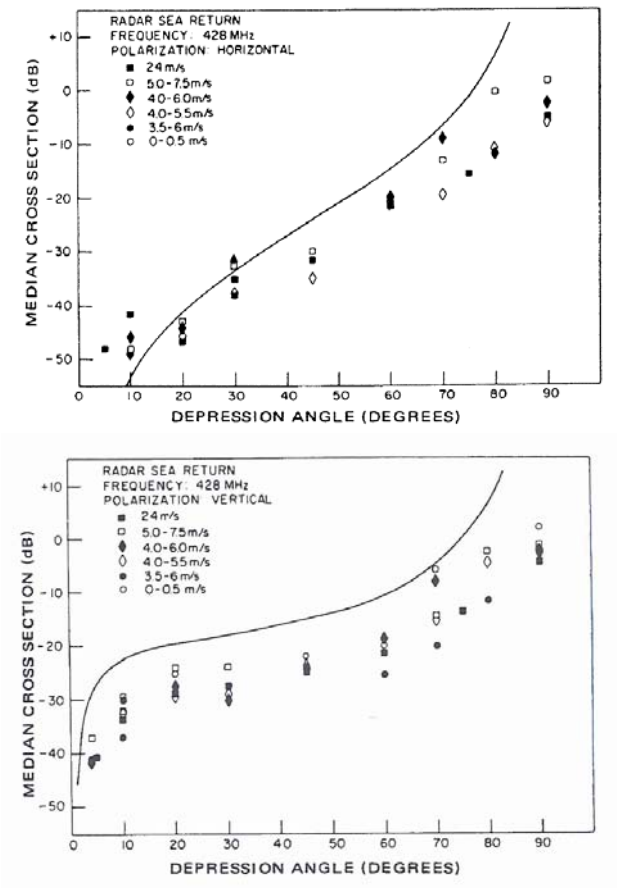

Figure 14: The variation of σ^0 as a function of the grazing angle (in the figure it is denoted as a depression angle) [27]

In that way, they manage roughly to assess the detection capabilities of such radar structure. The Barrick's work is one of the most cited works in this area. It gives normalized clutter RCS and an average scattered signal spectrum from a moving sea surface, based on a straightforward first-order hydrodynamic and electromagnetic analysis [5]. He also considers the polarization, grazing angle and frequency in VHF range (fig.13). A considerable work on this topic has been reported in [27], where

the normalized sea clutter RCS in vertical polarization is found to be greater than the horizontal ($\sigma^0_{VV} > \sigma^0_{HH}$). Figure 14 consists of experimental results, which also confirm this behaviour and elucidates the expected amounts of the sea clutter in the VHF range [27]. The ***low-grazing*** angles within this frequency range are characterized with σ^0 value lower than -50 ÷ -70dBsm [27]. The Nathanson sea clutter tables, gathering experimental data, are cited in [27]. The information from them, relevant to our goals, is summarized in fig. 15 for σ^0 near VHF frequency band and the vertical polarization, as a polarization of interest. It shapes a considerable picture for the range of the σ^0, depending on the wind speed, polarization, the grazing angles start from 5 degrees.

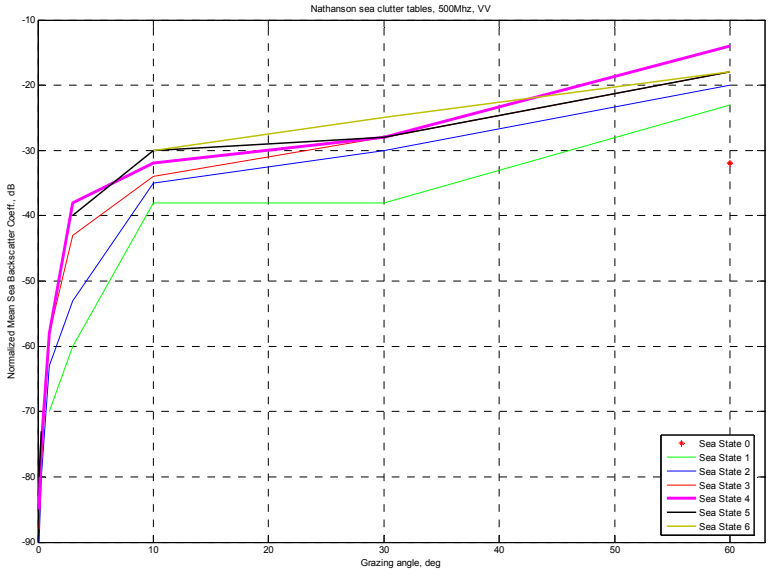

Figure 15: Graphical summary of the Nathanson tables. The variation of σ^0 as a function of the grazing angle [27,30], polarization VV, freq. 500MHz

Those tables include mean data from about 60 experiments. Although, Nathanson uses a monostatic radar and some of the results have 4-8dB error [27, 30], we can draw a good picture about our normalized clutter coefficient expectations, which also proves the Barrick's outcome.

The aforementioned is the main drawback of the sea clutter behaviour, measured in monostatic mode within frequency range. Due to various reasons (historical, easy description, undisputable measurement, complexity, etc.) the information for the monostatic clutter is more than the information in bistatic mode. Although, the Barrick's work is not for bistatic scenario, if a reasonable description of the clutter difference between the monostatic and bistatic mode exists in the literature, the clutter expected for P-AIS applications can be derived. The bistatic sea clutter features drawn from the literature investigation, helping to understand and build the bistatic clutter model are summarized as follows: *(i)* The clutter cell area for the resolution time-limited case at low grazing angles in the forward scattered direction is more than 30dB larger than in the backscattered, but is less than 10dB larger for azimuthal angles as large as 135^0 from the backscattered direction [41]. Here the azimuthal angle represents the angle in respect to the backscattered direction where the bistatic angle is zero [41]. *(ii)* The surface clutter radar cross section is significantly larger in the forward scattering direction than in backscattering, which may nullify any advantages of a possibly enhanced target RCS in forward scattering direction, particularly at frequencies larger than 300MHz [41]. *(iii)* The bistatic surface clutter returned at a bistatic angle as large as 45^0 is not appreciably different from that of the backscattered region [41]. *(iv)* Although various models (empirical, geometrical and statistical) of surface scatter are made, having the basis of various assumptions, considering the characteristics of the surface, meaningful results are difficult to achieve except over a relatively narrow range of elevation or out-of-plane angles [41].

Summarizing the aforementioned in this paragraph and the extensive research amongst the literature, we can conclude, that:

- Amongst the scientific literature, there is enough information about the normalized RCS sea clutter within VFH frequency mode. As it was expected, most of the data are for monostatic mode. There are several valuable works providing good relation between the monostatic and bistatic situation, which can be successfully used further in our analysis. We assume mean clutter difference between monostatic and bistatic mode about ±10dB (excluding the forward scattering mode).

4. Current project results

The extensive literature survey concluded that in order to have some reasonable idea about the potentiality of the energy distribution considering the passive AIS approach, the bistatic radar equation (eq.1) needs to be solved and the AIS wave form examined. The most powerful tool for study these capabilities is the Ambiguity function. Likewise, the main obstacles will be to have an idea about the potential target and clutter RCS within this VHF range. The literature survey gives more information about the clutter behaviour than the target RCS. Therefore the decision to perform several experiments in order to gather *RCSeff* in-situ results was made.

4.1 AIS Ambiguity function estimation

Figure 16 shows the unweighted ambiguity function $|\chi(\tau,\omega)|^2$ of a real AIS message that encodes information about the broadcasting source, including position, speed and course over ground [38]. The autocovariance function shows relatively good range ambiguity properties and the range resolution limitations of AIS waveforms. For this message, the peak to sidelobe level measure is 12.9 dB in range, and 13.2 dB in Doppler. The exact numbers will be related to the specific message, although the variations are expected to be small. This is a consequence of the time length and the modulation spectrum of the AIS signals as regulated by international standards [25]. According to the ITU recommendations [32], for the 25 kHz channel mode, the AIS signal spectrum shall be within the emission mask defined by -25 dBc at ± 10kHz and -70 dBc at ± 25 kHz from the centre frequency. This reduces the effective bandwidth, which is only a fraction of the channel bandwidth, and therefore the range resolution performance. By analyzing different AIS real broadcast signals, the P-AIS range resolution of approximately 20 km can be derived. Such monostatic resolution performance can be seen as the best case of the P-AIS system when considering a single bistatic pair. Using multiple illuminators mitigates the range resolution limitation, achieving smaller resolution cells depending on the multistatic topology under investigation.

From the considerations reported in [38], the monostatic Doppler resolution of the AIS signal is about 40 Hz, whereas the velocity of a ship gives Doppler shift within few Hz. This makes P-AIS predominantly a range-only application for maritime surveillance. Summarizing the aforementioned we might stress on:

- The ‘high’ setting transmitted power of 12.5 W yields a power density of around -78 dBW/m2 at 10 km and -84 dBW/m2 at 20 km considering a typical dipole gain of about 3 dBi. This is comparable to other illuminators of opportunity investigated in literature as summarised in [15].
- As commonly implemented in passive radar applications, ranging is achieved by matched filtering the signal coming directly from the illuminator into the ‘reference’ channel with the delayed replicas reflected by targets and recorded by the ‘surveillance’ channel. In some operational scenarios, P-AIS might be requested to deal with weak reflected signals. This urges for high-sensitivity receivers especially in the surveillance channel, where severe constraints on direct signal suppression are posed - the direct signal largely overlaps in time with the reflected echo. In principle, the surveillance signal might contain residuals of the AIS direct signal, which can be only suppressed by exploiting signals’ spatial diversity at antenna level. Follows correlation with the direct signal – collected by the reference channel. Accurate Time Difference of Arrival (TDOA) estimation might be achieved with Generalized Cross Correlation (GCC) techniques, which are expected to fully exploit the knowledge of the spectral characteristics of the AIS signal, or Maximum Likelihood Estimation (MLE) techniques – well known for working in multipath-affected operations.

- Because the direct Doppler resolution of the AIS signal is very low, the time properties of the signal are not destroyed within the whole available target velocity range, which makes this signal very suitable for time analysis.

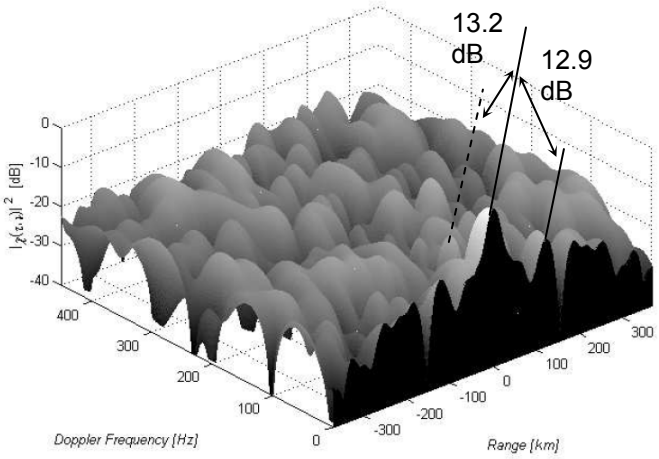

Figure16: Ambiguity function of a real AIS signal [38]

4.2 Experimental Target RCS estimation

Due to the conclusions made in §3.1 we assume that the monostatic target RCS is our "base" of estimations. Because, in our experiments, we have specific propagation factor, and this factor also is a part of the radar equation, our measurement of RCS will be the effective monostatic RCS (*RCSeff* monostatic). Firstly, the limits for the critical grazing angle are defined, in order to simplify the pattern propagation factor, mainly due to specular reflection (the case of reflectivity from smooth surface). Equation 5 is used in order to evaluate the critical grazing angle according to the theory. There are several sea states reports, one of the most well known is the Beaufort scale. The Beaufort scale gives 13 sea state numbers to which corresponds 13 values of the sea roughness (some sources give 17 states) [20]. This scale matches the sea state with wind speed, mean value of the sea wave h_{rms}, etc. The mean value of the sea wave is particularly important for the measurements, because it is related to the definition of the roughness in terms of the radio wave propagation (fig.3).

In [28] another approximate expression about the sea state is given through h_{rms}:

$$h_{rms} \approx 0.025 + 0.046 S_{state}^{1.72} \qquad (16)$$

The following table describes our estimations about the critical grazing angle according to eq.5 and eq.15 and the Beaufort scale from 0-9 :

Table 1

Sea state	0	1	2	3	4	5	6	7	8	9
A h_{rms}, m (Beaufort wind scale) [7]	**0,003**	**0,027**	**0,09**	**0,21**	**0,42**	**0,72**	**1,14**	**1,7**	**2,43**	**3,33**
A ψ_{gc}, deg	**~90**	**~90**	**~90**	**~90**	**~90**	**38,7**	**23,3**	**15,4**	**10,7**	**7,8**
B h_{rms}, m (eq.16)	*0,025*	*0,071*	*0,177*	*0,33*	*0,524*	*0,758*	*1,028*	*1,332*	*1,67*	*2,039*
B ψ_{gc}, deg	*~90*	*~90*	*~90*	*~90*	*59,1*	*36,4*	*26*	*19,8*	*15,6*	*12,8*

For conservative reasons we evaluate both expressions for mean roughness and take the smallest values. It is seen that the critical angle for this frequency is within very large sea state range. Hence, if we consider maximal expected grazing angle 23 deg. and VHF range, according to the theory, the sea may be considered as a flat (smooth) surface between moderate and strong breeze conditions (Beaufort scale 6). In order to measure the *RCSeff*, we use small radar based on Programmed Network Analyzer (PNA) [13, 18, 1, 2]. The additional details about the *RCSeff* experiments, the parameters, frequency band, antenna pattern and the algorithm of dynamically *RCSeff* extraction [10] are given in appendix 3 and 5. Two scenarios and several types of targets are considered. The experiment scenarios are shown on the next figure. We define two scenarios: ***scenario 1: low grazing angle*** (antenna height h=22m)

and ***scenario 2: extremely low grazing angle*** (antenna height h=3m), the maximal grazing angle is less than 23 deg. Therefore the assumption for pure smooth ground reflection in the following experiments is plausible.

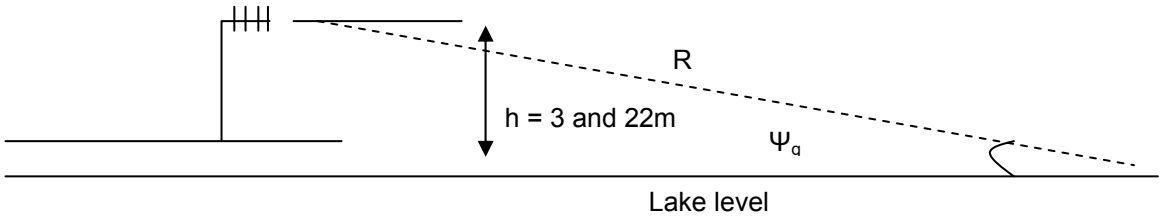

Figure 17: Experiment scenarios

The target types are: type 1 – ferry, type 2 – motor yacht, type 3 - small wooden boat. Their detailed explanation is given in appendix 4. In the experiment, the start frequency is: 146 MHz, stop frequency: 176MHz; 1601 frequency points. Different polarization is used. As results, some values of *RCSeff* at different ranges are estimated in order to estimate the *RCSeff* behaviour. We assume that the major dependence of the *RCSeff* from the range is due to: *(i)* the antenna propagation factor phenomenon; *(ii)* the changing aspect angle of the target illumination; *(iii)* the relative target position within the antenna beam shape. In our result justification the target aspect angle changing is neglected and focused mainly on the antenna pattern propagation factor and the relative position of the target and the antenna beam shape (*ii* and *iii*). For example, if we consider the used antenna diagram, shown in appendix 3, a straight line crossing target gives 1dB variation. If the target crosses the beam diagonally, as it is done in more of the experiments, the difference could be 3-4 dB. Likewise, we are aware of the factors as change of the beamwidth from the near standing objects, shadowing effects, second order reflection (for example transmitting antenna-object-target-receiving antenna) etc. Due to those obstacles the measurement of the *RCSeff* is not precise, but we can use the results as really obtainable values of maritime targets. In order to picture the shape of the pattern propagation factor influence, the two ray propagation model is estimated (fig. 4) [7]. Smooth reflection from water surface is considered. Taking into consideration figure 18 it is obvious that the extremely low grazing angle scenario decreases the energy constantly as a function from the range. Whereas, the low grazing angle scenario has some fluctuations of the resulted gain, which might directly affects the measurements, especially between 200 and 300 meters.

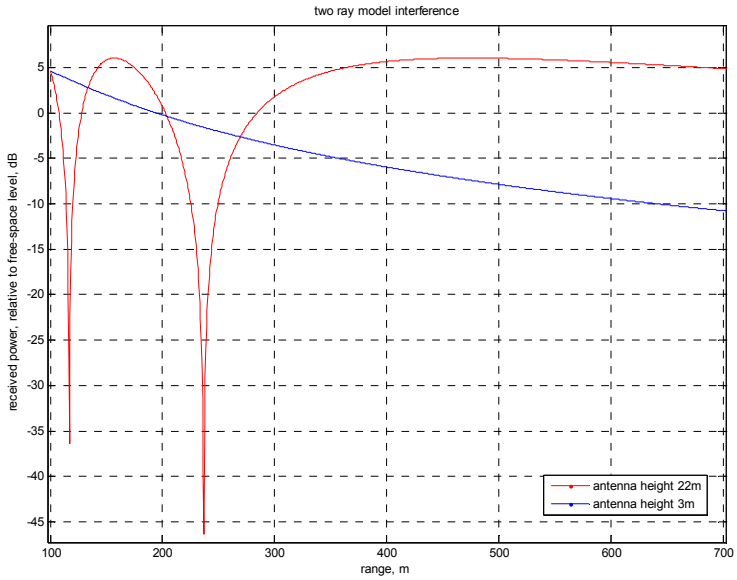

Figure 18: Two ray interference

4.2.1 Scenario 1

Figure 19 describes schematically the experimental field deployment for scenario 1 and the possible tracks of the explored targets. The tracks are constructed after the data analysis, taking into consideration the usual behaviour of the vessels on the experimental field. The tracks 1 to 4 and 6 are the approximate ferry path, whereas track 5 is a track going towards the yacht port

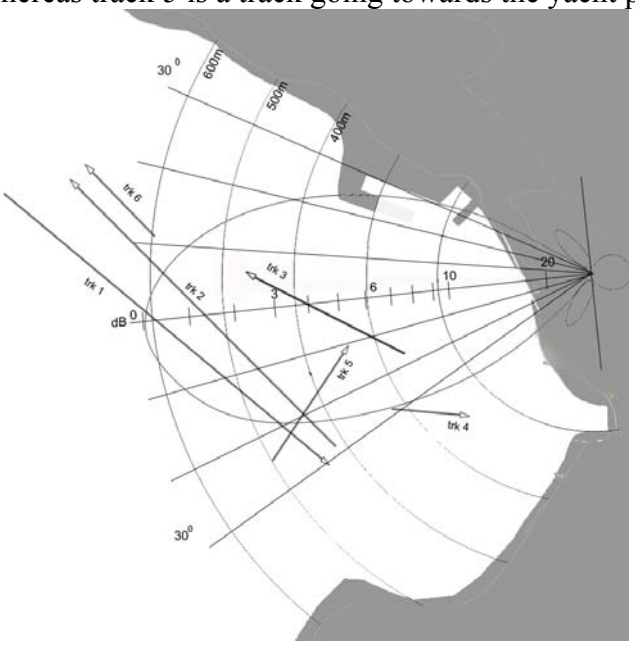

Figure 19: Scenario 1 diagram, antenna height 22m

Figure 20 presents the first studied target track. According to the two ray model interference at this range the received power is almost constant value (fig.18). Therefore, the behaviour of the *RCSeff* can be explained in terms of a diagonal beam track crossing. The target becomes visible at a range about 700 – 800 m and crosses the antenna beam at an angle of about 30 deg respecting to the pointing direction, which gives about 20 dB decrease of the antenna gain (fig.19) respecting the maximum. Then the *RCSeff* increases until the target reaches the maximum of the antenna beam at about 550m. Moving forward the measured *RCSeff* decreases to a difference about 20dB at the 30 deg at the end of the observation period.

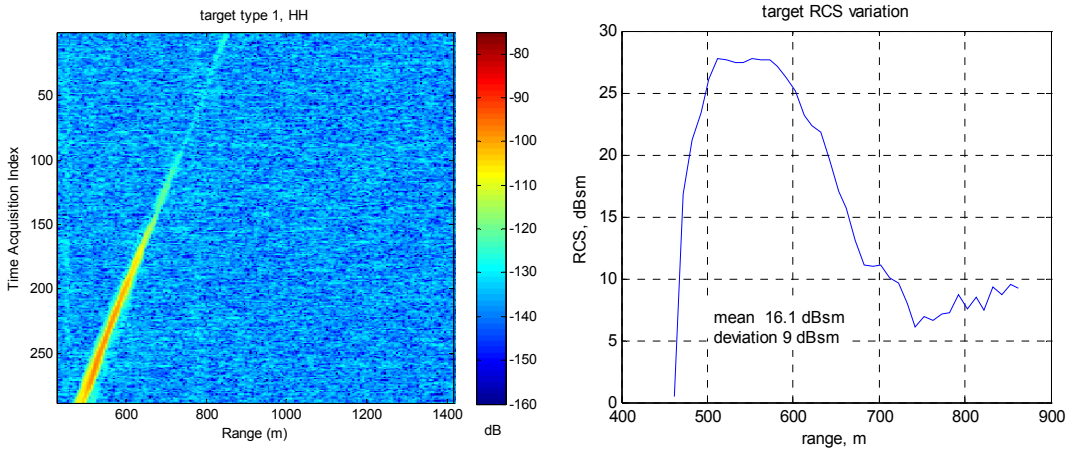

Figure 20: Scenario 1, track 1

Figure 21 describes track 2, which moves slowly away. The target is a type 1, i.e. a ferry with "Π" shape car compartment and this may explain the presence of a "doubled" track and the notch of the *RCSeff* at about 700m possibly due to a destructive effect at the aspect angle change. Likewise, the begin and end of the track follow the behaviour of diagonal antenna beam crossing.

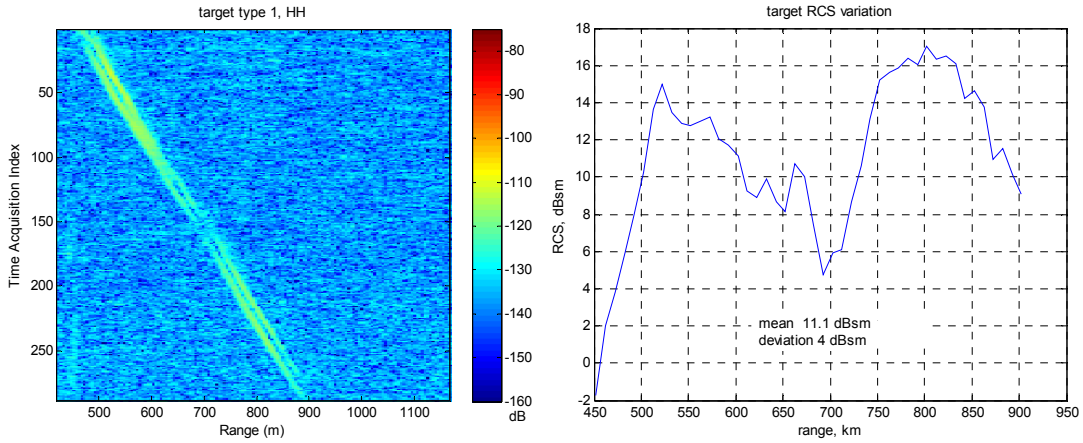

Figure 21: Scenario 1, track 2

The track in figure 22 moves away passing the antenna pointing direction at about 350m and showing a behaviour of *RCSeff* similar to figure 20. The effect of the two ray propagation model should be considered to explain the behaviour below 280 m distance.

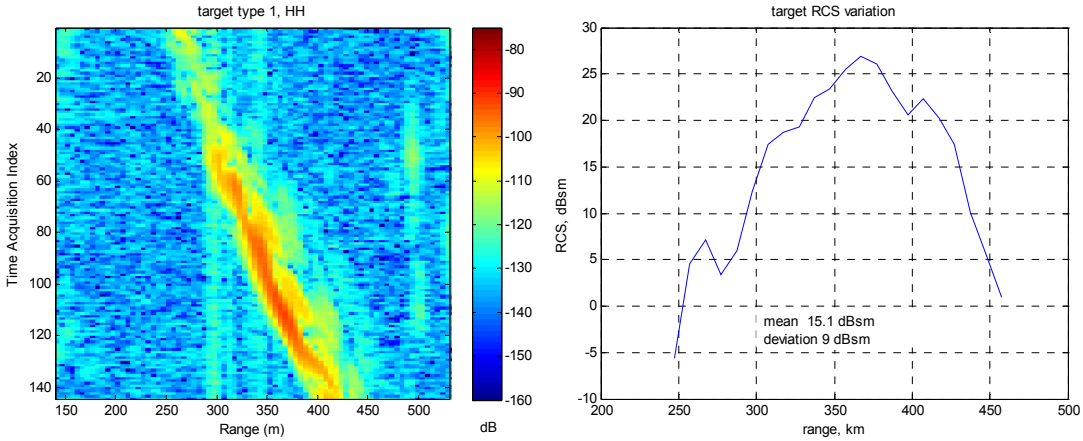

Figure 22: Scenario 1, track 3

Track 4 is a short record moving more than 30 deg. towards the antenna pattern and the attenuation is higher. Track 5 is a diagonally approaching yacht contributing difference of about 5dB due to its position within the antenna pattern. The moving away ferry (track 6) is a subject of the same effect, as well.

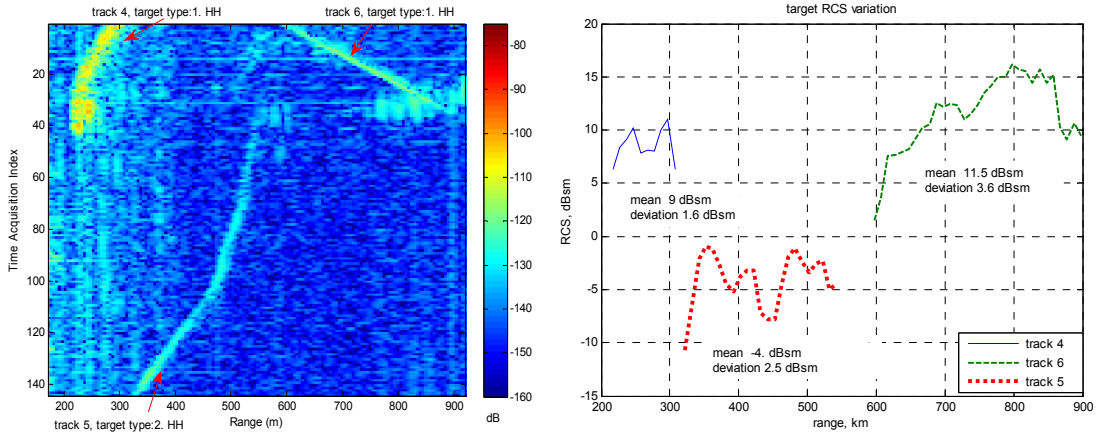

Figure 23: Scenario 1, tracks 4 - 6

4.2.2 Scenario 2

Scenario 2 is schematically described in figure 24. The antenna height is 3m positioned on the coast line causing extremely low grazing angle conditions. Here the two ray model (fig.18) gives constant decrease of the field strength as a function of the target distance. For example, a decrease of 5dB at 200m, 10dB at 400m etc. should be considered. Figure 25 represents two cross passing ferries. The *RCSeff* behavior is similar, but track 2 has "worse" position in the antenna pattern or smaller ferry [23]. The maximum result of track 1 scenario 2 is 10dBsm at about 300m. According to figure 18 there is of 10dB attenuation, the antenna pattern position gives 6dB loss. If the losses are compensated the maximum would be about 26dBsm, which is comparable with the maximal value of figure 20. Track 3 is also a ferry giving results similar to track 1 and 2.

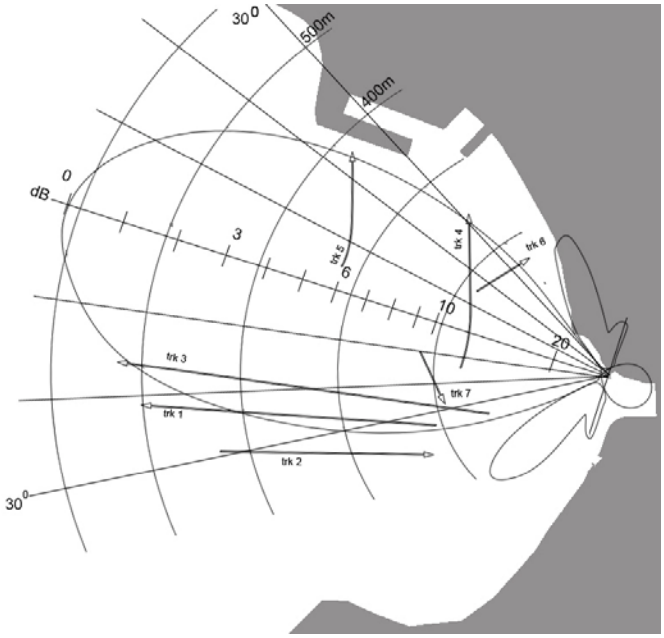

Figure 24: Scenario 2 diagram, antenna height 3m

Track 4 and 5 belong to a yacht and show a similar behaviour. Track 4 has maximal value of about 6 dBsm, whereas track 5 has 3 dBsm. Because the target distance is different, the difference in the maximal values can be explained by the propagation factor phenomenon (fig.18). Track 6 and 7 are small wooden fishing boats, diagonally approaching towards the antenna. In these cases, data are insufficient to study the *RCSeff* behaviour in details. Nevertheless, it is interesting to note their detectability.

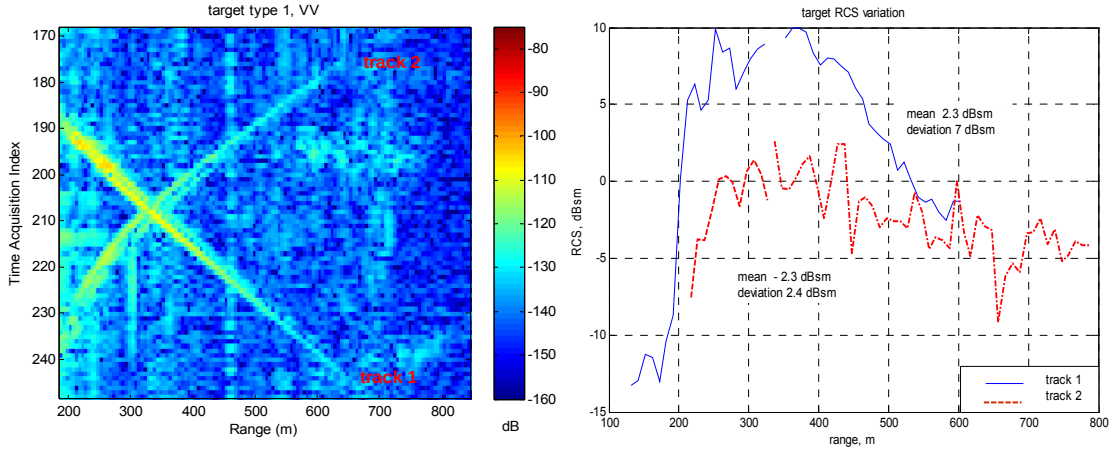

Figure 25: Scenario 2, track 1 and 2

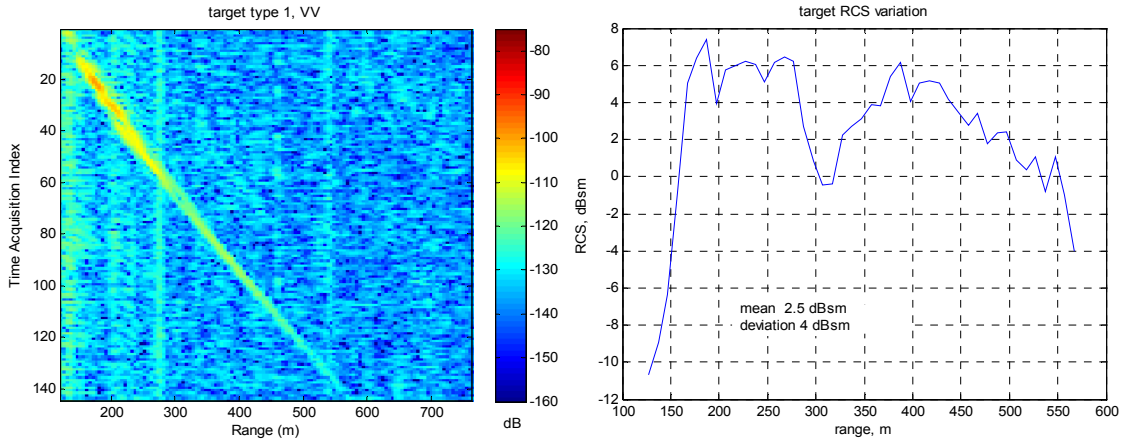

Figure 26: Scenario 2, track 3

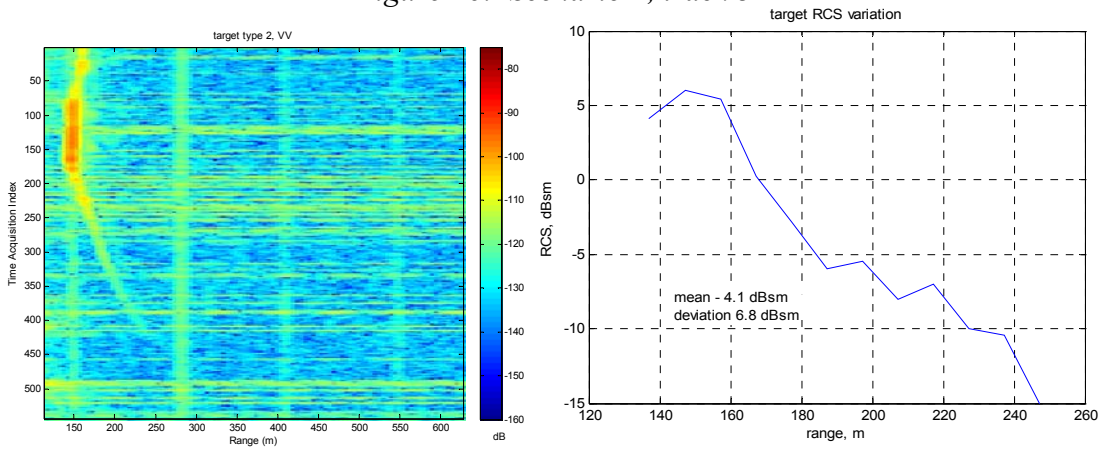

Figure 27: Scenario 2, track 4

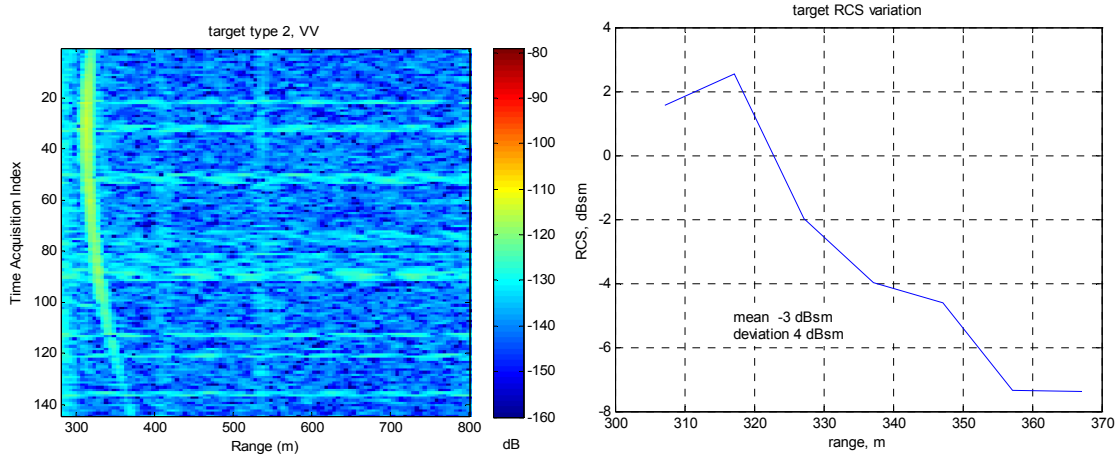

Figure 28: Scenario 2, track 5

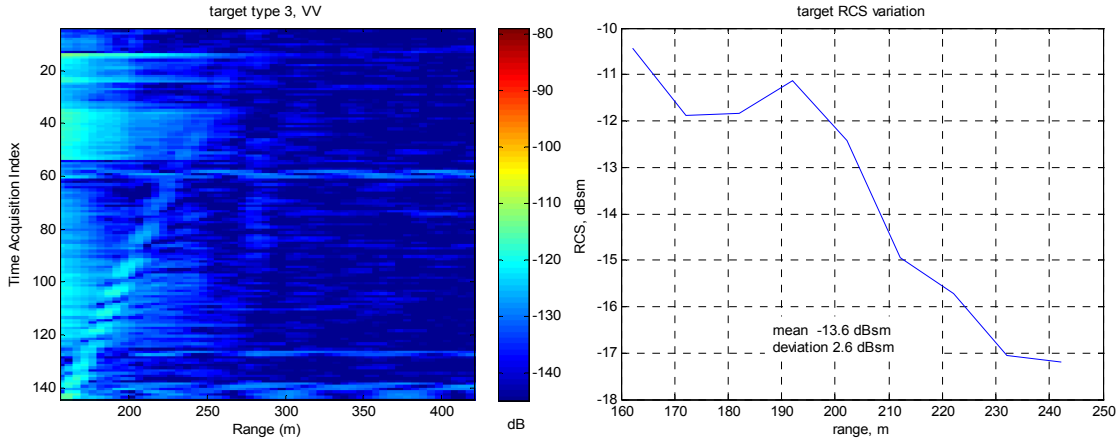

Figure 29: Scenario 2, track 6

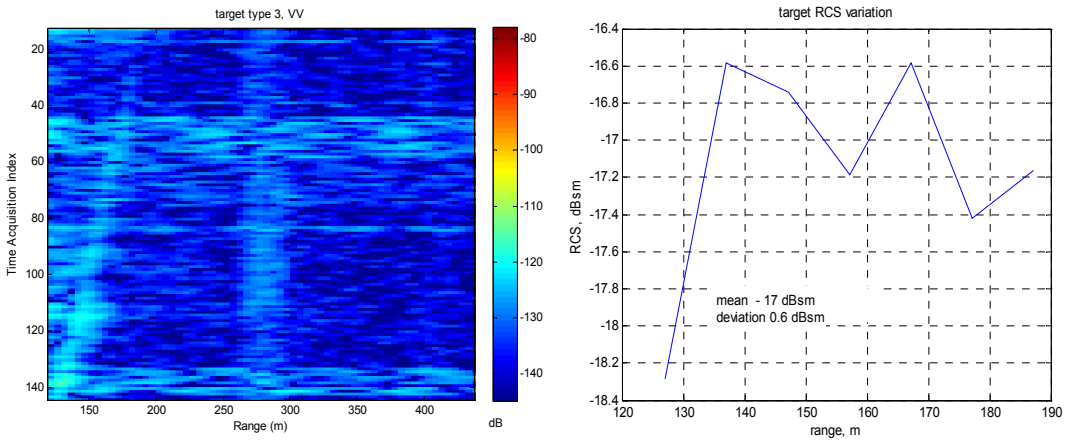

Figure 30: Scenario 2, track 7

Summarizing the results above, we can conclude that the targets are clearly visible in those frequencies; even the small wooden boat can be distinguished without additional sophisticated signal processing of the radar data. The *RCSeff* of the different targets depends of the target range, due to the antenna pattern and propagation factor reasons. Furthermore, the low grazing angle experiment provides visibility of larger distances. On the other hand, the exploitation of the extremely low grazing angles should be used, taking into account that the reflection from the water surface might decrease the antenna gain along the water surface. The variation of the *RCSeff* results also from the different target shape and its orientation towards the radar. The large variation of the sea state, within a smooth sea surface is considered, could be advantage, because according to the theory in the smooth sea surface the clutter is more predictable and depends mainly on the grazing angle but not on the sea roughness.

4.3 Clutter assessment

In our experiments the clutter measurement is complex and ambiguous. Because the water state was calm and the radio wave was considerably large (VHF range), the water surface is considered as a radio wave mirror (smooth reflection). The experiments are conducted with maximal antenna height near 22m and the expecting grazing angles are less than 4 degrees. The literature survey shows the very low clutter values for this grazing angle and VHF frequency (see §3.2). We assume that the received signal from distance large enough to reduce maximally the influences of the antenna coupling, the close reflections from the coast line and the sidelobe leakage is hardly distinguishable from the received noise. In other words, it is subjected on the Rayleigh distribution or there is no dominant component of the background scatterer, so that component will have zero mean and phase evenly distributed between 0 and 2π. In order to verify this, we assess the amplitudes and phase distribution over profiles in range containing neither targets nor land areas.

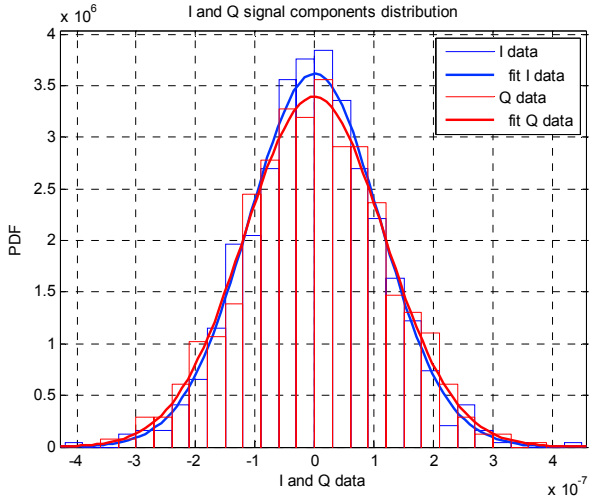

Figure 31: Distribution fitting result for I and Q signal components

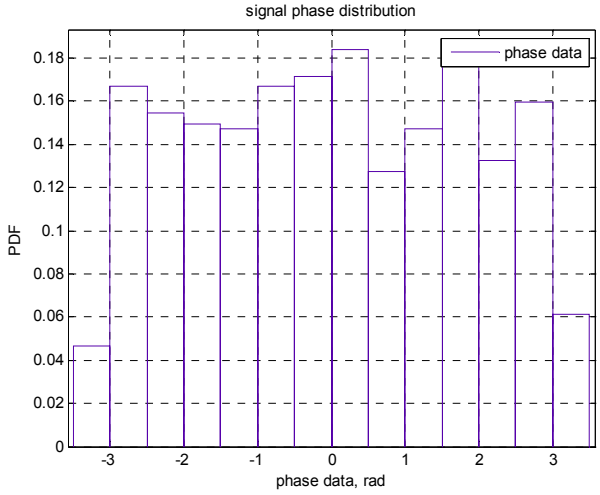

Figure 32: Phase distribution in degrees between the I and Q signal components

Figures 31 and 32 reveal the behaviour of a tested sample. Based on those figures we conclude that the clutter measurement in this case is very hard and mainly white Gaussian noise is received. Taking into consideration the aforementioned in §3.2, literature clutter values will be used further.

4.4 Coverage Prediction Tool

Our substantial goal after the aforementioned results is to develop a model, which might shape the P-AIS system energy coverage. The model is based on the complete radar equation and will include the maximal possible number of parameters in order to model it reliably. The used equation is based on the eq.15,

$SIR = \frac{1}{\frac{1}{SNR} + \frac{1}{SCR}}$, where *SNR* and *SCR* are derived from eq.1 and eq.14 and encompasses the influence of the SNR and SCR, which is summarized in the term Signal to Interference Ratio (SIR).

$$SNR = \frac{\Pr}{Pn} = \frac{PtGtGr\lambda^2\sigma_b F_t^2 F_r^2 G_p}{(4\pi)^3 Rt^2 Rr^2 LkT_0 BF} \text{ (eq.1) and } SCR = \frac{\sigma_t}{\sigma_c} = \frac{\sigma_t}{\sigma^0 Ac} \text{ (eq.14)}$$

According to the AIS specifications the parameters are as follow [32, 19]: *Pt* – the transmitter power = 12 in *Watts*; *Gt* – the gain of the antenna transmitter, 3 *dBi* /the VHF antenna is considered as a monopole/; λ – the radar wavelength, *meters*, where $\lambda = c/f$, *c*- the velocity of the light, *f* – standard AIS frequency 161.975*MHz* and 162.025*MHz* [32,19]; k – the Boltzmann's constant, 1.38065*10^(-23); T_0 – noise reference temperature, 290 *K*; *B* – the receiver bandwidth, 25*kHz*; *F* - the receiver noise figure, 5*dB*; *L* - the total loss from transmitter-target-receiver, 5*dB*; Gp – processing gain for 0.25*sec* is 38*dB* (eq. 1a). The AIS package duration according the AIS specifications is 25*ms*. The maximum possible processing gain can be used (eq. 1b), because the maximal target boat acceleration for radio package duration of 25*ms* is about 29.6 m/s^2, which is beyond the possibilities of the contemporary fleet.

Bistatic situation, under study, consists of omni-directional transmitting antenna (the ship antenna) and a directive four element receiving antenna array with gain **18.7 dBi (**the pattern shown in appendix 3**).** Because the passive AIS system is at least bistatic system (the transmitter and receiver are spatially distributed), the bistatic radar equation is used for mathematical description of the energy characteristics of such a system (eq.1). As mentioned above, this equation describes the energy received in the sensor considering the system parameters (§2.1). Based on the bistatic radar equation, a MATLAB tool is developed. It is preliminary verified with previous works [15, 17]. Considering the communication purposes of the AIS and the passive AIS concept [32,19] (the transmitter cannot be

controlled and the antenna is a dipole with omni-directional radiation pattern,) a typical passive AIS scenario has specific footprint geometrical configuration (fig. 33).

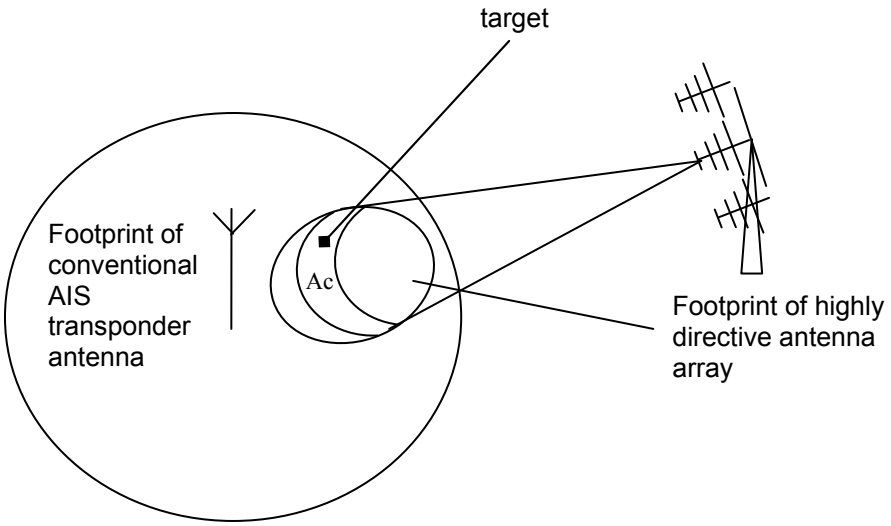

Figure 33: Geometry of a passive AIS configuration and receiving antenna footprint

Therefore, the advantage of reducing the cell range resolution area as a cross-section of two antenna beam pattern is not possible (fig. 8). The coverage prediction tool is based on eq.15, which derives from the radar equation (eq.13) and includes the clutter influence (eq.14). The footprint peculiarities, the power parameters of the AIS system, the antenna pattern (fig. 33), the bistatic geometry, the *RCSeff* and the clutter model (§3.2) are the input of the coverage prediction tool. As it was concluded in §3.1, the lack of data for RCS of different targets exactly within VHF frequency range and the comparison between bistatic and monostatic target RCS allows using the in-situ real monostatic *RCSeff* measurement (§4.2) as parameters in the coverage prediction tool. According to the conclusions about the low values of the normalized sea clutter value (see §3.2) and its difficulties to be measured by our sets, the normalized clutter RCS as a function from the grazing angle is modelled according to the Barrick's work [5]. The equation 10 estimates the antenna footprint area Ac. The SCR and SIR are taken into consideration according to the eq.14, 15.

This work does not contradict with the measurement conclusions (§4.3) and the other reported results (see §3.2). The function of the normalized sea clutter RCS from the grazing angle is also considered as a parameter in the prediction tool.

Next pictures evaluate eq.1 including: SNR and SCR estimations and the measured values of the effective maritime target radar cross sections. The purpose of this evaluation is to give an idea about the coverage range in passive AIS scenario considering the most important factors as: clutter influence, grazing angle influence, target radar cross section and the pattern propagation factor. Two scenarios are used and different bases between the transmitter and receivers are taken into consideration. Both scenarios, defined in §4.2, ***scenario 1: low grazing angle*** (antenna height h=22m) and ***scenario 2: extremely low grazing angle*** (antenna height h=3m) are considered. The pattern antenna propagation factor is included in the measurement of the *RCSeff* (see §2.4).

Figure 34 shows the signal-to-noise ratio between AIS transponder transmitting at maximal power and a receiver deployed at 10km distance. The *RCSeff* is 22*dBsm*. The figure presents the behaviour of eq.1 without the clutter influence. It can be seen the good detection signal-to-noise ratio coverage and the shape of the Cassini ovals. On the other hand, next figures (fig. 35-40) are constructed considering the clutter contribution (acc. eq. 15) and the peculiarities of the passive AIS configuration (described in fig. 33). The figures present the behaviour of eq.15, which includes eq. 14, eq.1 and the grazing angle clutter dependency. The constant SNR zones shape changes as a difference from the Cassini figures. It can be observed that there is only one zone candidate for possible detection

– the receiver zone. This is due to the increase the range cell area as a function of the distance from the receiver (fig.33).

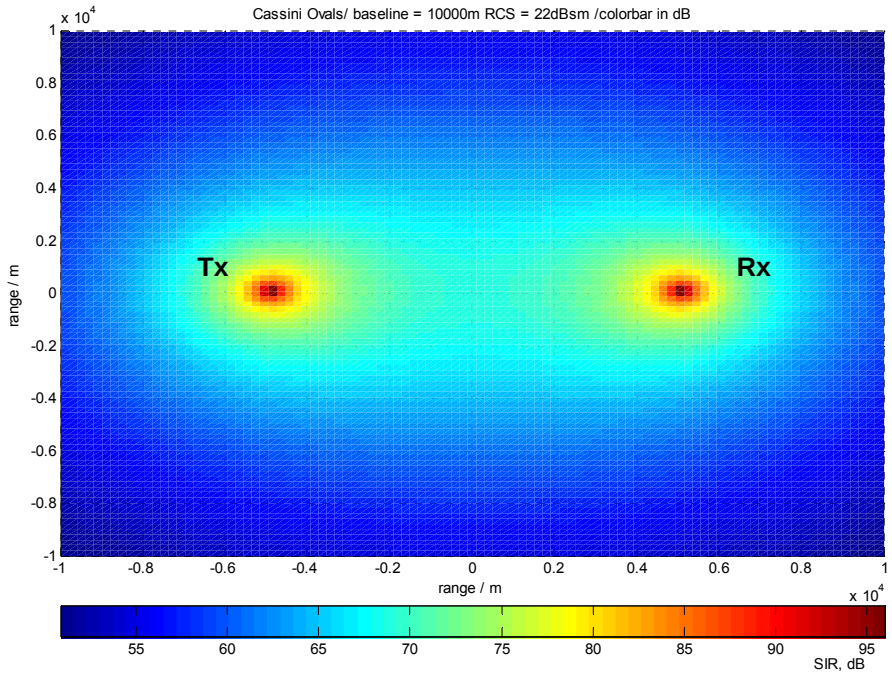

Figure 34: Signal-to-Noise Ratio bistatic contour for baseline 10km and RCSeff = 22 dBsm, no clutter influence, scenario 1

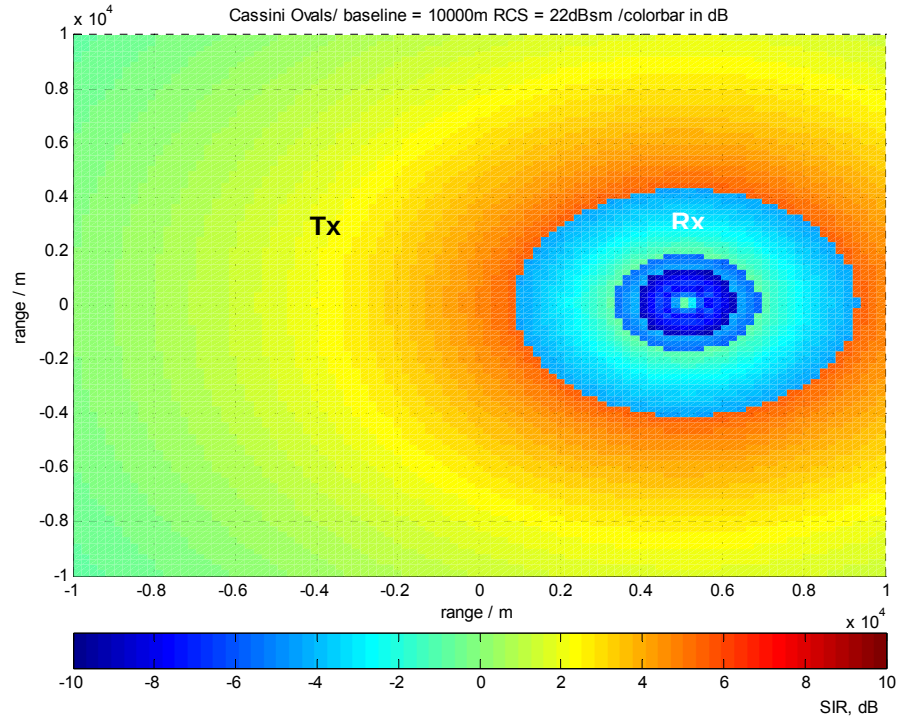

Figure 35: Signal-to-Interference ratio bistatic contour for baseline 10km and RCSeff 22dBsm, scenario1

Thus, the clutter influence augments when the distance from the receiving point increases. On the other hand, Signal-To-Interference-Ratio (SIR) decreases close to the receiver, because the grazing angle increases. This effect does not contradict to the theory [7]. Figure 35 and 36 depict the returned

signal-to-interference ratio for data taken from experiment in figure 20. The *RCSeff* is about 22dBsm (target 1 max value), antenna height is 22 m and the distance between transmitter and receiver 10km.

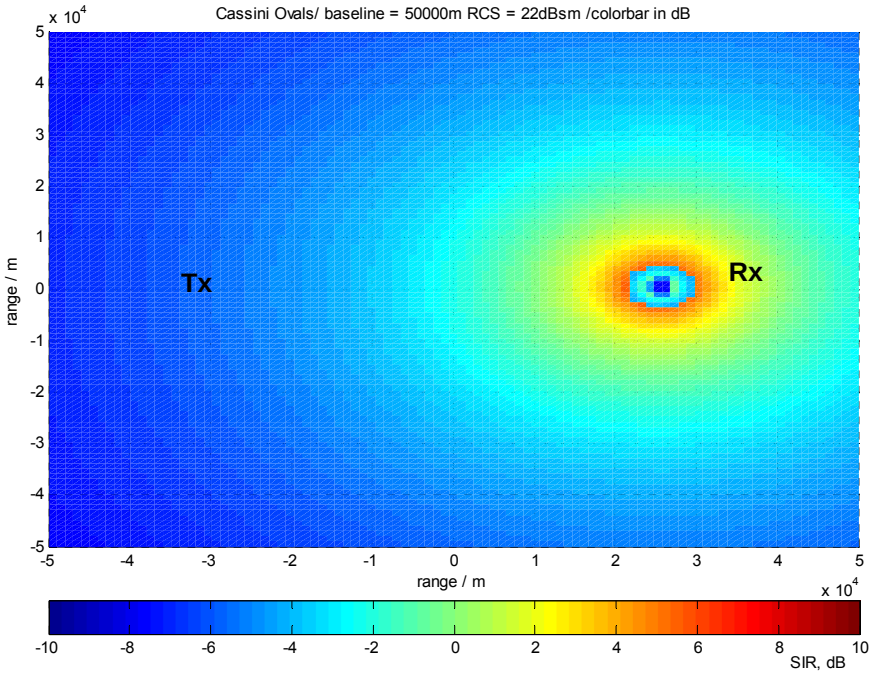

Figure 36: Signal-to-Interference ratio bistatic contour for baseline 50km and RCSeff 22dBsm, scenario 1

Figure 36 shows the picture in bigger range – 50km distance, which reveals similar behaviour of the signal-to-interference ratio. If we follow the 5dB points we can see that 20km coverage is possible and to conclude that long distance coverage is very well represented for this low grazing angles about 2-4 deg. Figure 37 is made for lower *RCSeff* 13dBsm and base of 10km. As expected the returned signal-to-interference ratio is about 10dB lower than the previous cases.

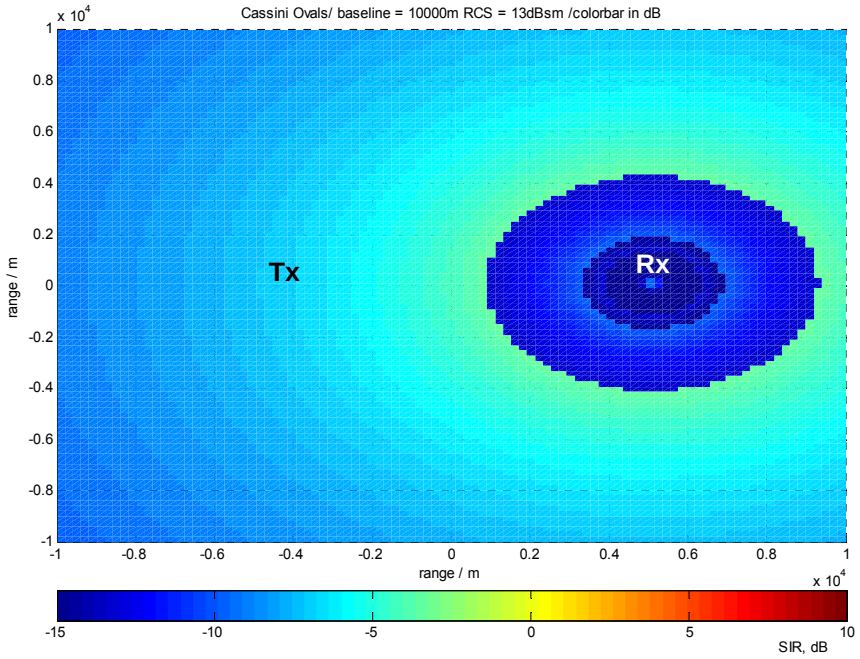

Figure 37: Signal-to-Interference ratio bistatic contour for baseline 10km and RCSeff 13 dBsm, scenario 1

Figure 38 uses the *RCSeff* data from extremely low grazing angle experiment - scenario 2 (§4.2 figure 17), track 1, fig 25, naturally due to the low *RCSeff* the SIR is little.

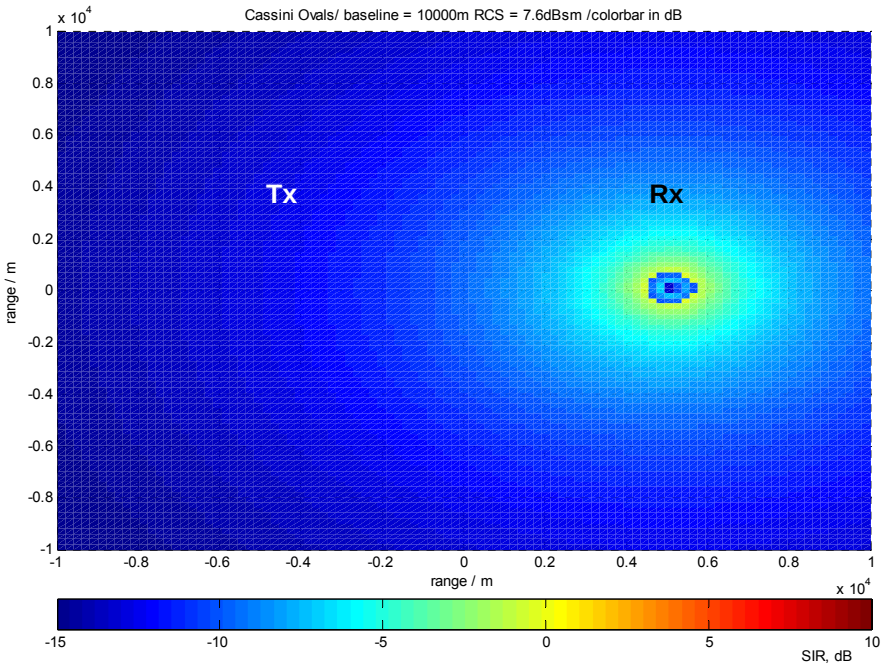

Figure 38: Signal-to-Interference ratio bistatic contour for baseline 10km and RCSeff 7.6 dBsm, scenario 2

Figure 39 estimates the influence of the grazing angle. A target considering 22dBsm *RCSeff* is put into the coverage prediction tool in extremely low grazing angle conditions. In other words, fig. 39 describes what would be the difference for a given target neglecting the pattern propagation factor, and considering the clutter dependence from the grazing angle only (eq. 15). In comparison with fig. 35 it is clearly seen that the extremely low grazing angle conditions give better coverage in proximity to the receiver due to the low clutter influence.

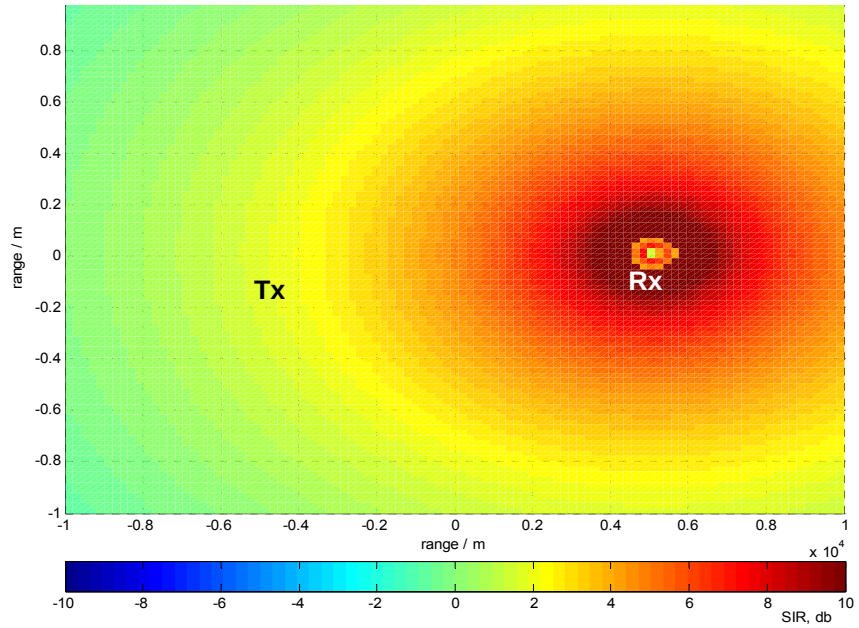

Figure 39: Signal-to-Interference ratio bistatic contour for baseline 10km and RCS 22dBsm, scenario 2

In the practice, such influence of the pattern propagation factor can be mitigated through specifically designed antenna pattern. Taking the advantage of the extremely low grazing angle in the receiver proximity is plausible by a specific antenna. On the other hand, the extremely low grazing angles decreases the detection horizon due to the natural Earth curvature. Therefore, an operational P-AIS system should encompass a trade-off solution between the antenna pattern designs and the antenna height.

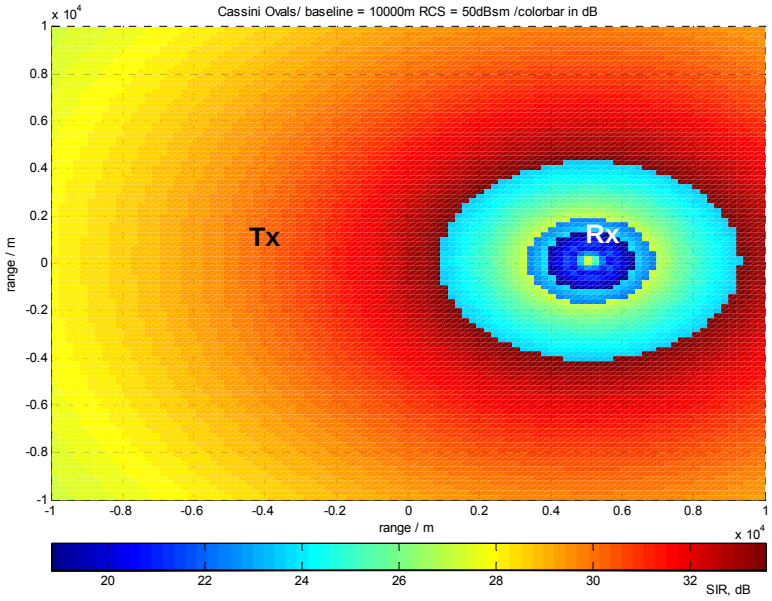

Figure 40: Signal-to-Interference ratio bistatic contour for baseline 10km and RCSeff 50dBsm, scenario 1

Finally figure 40 reveals how the P-AIS coverage might appear if the *RCSeff* has 50 dBsm, which is also possible (§3.1). The area around the base line is completely covered with SNR more than 20dB.

Because the clutter origin, variation and the corresponding propagation factors are not well studied, the assessment of the target range in a background of clutter is one of the most difficult calculations in term of accuracy [7]. Considering the large cell area, the power of the clutter is dominant, and this can be easily proven. The larger the receiving antenna footprint is, the higher the clutter contribution is. Thus, eq.15 is mainly driven by SCR [34 pp.1.10]. Those results give a perspective view about the possible SNR relations and the target detectability performance for P-AIS application.

The main conclusions in this paragraph are summarized as:

- If we consider an ordinary detection SNR=10dB and define medium vessel as a target having *RCSeff* 50 dBsm, the power of the AIS transponder is enough to cover very large areas and detect medium to large vessels.
- The Passive AIS application peculiarities convert the equidistant SNR areas from Cassini shape into one possible detection oval SNR zone, centered at the receiver position.
- Extremely low grazing angles give better coverage in the receiver proximity, because the clutter influence is lower. On the other hand, those angles destroy the antenna pattern which decreases the range coverage. In order to exploit extremely low grazing angles the receiver antennas pattern should be particularly designed.
- The clutter contribution is fundamental and represents the main obstacle that might be faced.

5. Conclusions and Future work plan

This work described the main achievements in the Passive AIS (P-AIS) project. After an extensive literature research, in order to estimate the reliable values of target and clutter reflectivity at AIS frequency range, in-situ experiments were performed. An average *RCSeff* of several targets was estimated. Based on the preliminary results, found in the literature, and the additional estimations from the experimental results, a model of the normalized clutter RCS as a function of the grazing angle for the aforementioned experiments was adopted. The AIS signal waveform was analyzed and the potential range and Doppler resolution of the waveform was defined. A coverage prediction tool based on the bistatic radar equation, bistatic geometry theory, *RCSeff* results and published clutter data was created. Through the tool, the possible coverage area in using P-AIS approach, for several maritime target sizes, was assessed. The outcoming results confirm that in the VHF the sea surface can be considered smooth, even in case of high sea state. The different grazing angles have different coverage range. Without considering the clutter influence, the "visibility" of the target could be very good, basically within the whole line of sight. The passive AIS scenario, including one omni-directional antenna increases the negative clutter influence on the SNR at the receiver. In order to solve this high clutter contribution additional research steps should be explored:

- *Signal-to-Interference ratio improvement techniques*: *(i)* coherent integration of several messages from different AIS sources (the slow time of acceleration of the ships reveals great opportunity for such integration); *(ii)* non coherent integration techniques;
- *Techniques to mitigate the cell area and the clutter contribution: (i)* highly directive receiving antenna. *(ii) MIMO approach* – using many AIS transponders for detection; *(iii)* using extremely low grazing angles and specifically designed antenna pattern;

The present study and the developed coverage prediction tool can contribute to the better understanding the radio signal behaviour in the VHF range and can be applied in elaborated simulation software for research and development of secondary applications for the AIS.

6. Literature

1. Agilent "Radar Measurements", <http://cp.literature.agilent.com/litweb/pdf/5989-7575EN.pdf>
2. Agilent, "New Network Analyzer Methodologies in Antenna/RCS Measurements:
3. Ashwal W.A. Al-, C.J. Baker, A. Balleri, H.D. Griffiths, R. Harmanny, M. Inggs, W.J. Miceli, M. Ritchie, J.S. Sandenbergh, A. Stove, R.J.A. Tough, K.D. Ward, S. Watts and K. Woodbridge, "Statistical analysis of simultaneous monostatic and bistatic sea clutter at low grazing angles", Electronics Letters, vol. 47 No.10, May 2011
4. Averyanov V., "Multi-positioned radar systems", Minsk, 1978, in Russian
5. Barrick D. E., "The interaction of HF/VHF radio waves with the sea surface and its implications", Electromagn. Sea, AGARD Conf. Proc., pp.18-1 - 18-25 , 1970.
6. Barton D., „Radar Technology Encyclopedia", Artech House, 1998
7. Barton D., "Modern Radar System Analysis", Artech House, 1988
8. Barton D., W. F. Barton."Modern Radar System Analysis, Software & User's Manual", Artech House, London, 1991
9. Borek R., RTO-AG-300-V14. 19A - 1. Chapter 19A – RADAR CROSS SECTION.
10. Currie N.,"Radar Reflectivity Measurement:techniques&applications", Artech House, 1989
11. Domville A.: 'The bistatic reflection from land and sea of X-band radio waves'. Part I: Memorandum SLM1802, July 1967; Part II: Memorandum SLM2116, July 1968, GEC Electronics Ltd, Stanmore, UK
12. Dzvonkovskaya A., H. Rohling, "Cargo ship RCS estimation based on HF radar measurements", Proceedings of the International Radar Symposium (IRS'2010), Vilnius, Lithuania, June 16-18, 2010, Vol.1, pp. 160-163.
13. Galati G., "Advanced radar techniques and systems", Peter Peregrinus Ltd, 1993
14. Griffiths H. D., "Bistatic and Multistatic Radar", Military Radar Seminar, 7th September, 2004,
15. Griffiths H. D., and BAKER, C.J., "Passive coherent location radar systems. Part 1: performance prediction", IEE Proceedings on Radar, Sonar and Navigation, 152, Issue 3, pp: 153-159, 2005.

16. Griffiths, H. D., Al-Ashwal, W. A., Ward, K. D., Tough, R. J. A., Baker, C. J., Woodbridge, K. (2010). Measurement and modelling of bistatic radar sea clutter. Radar, Sonar & Navigation, IET DOI - 10.1049/iet-rsn.2009.0124 4(2), 280-292
17. Griffiths, H. D.; Long, N. R. W., "Television-based bistatic radar", IEE Proceedings, Part F - Communications, Radar and Signal Processing (ISSN 0143-7070), vol. 133, pt. F, no. 7, Dec. 1986, p. 649-657.
18. http://cp.literature.agilent.com
19. http://en.wikipedia.org/wiki/Automatic_Identification_System
20. http://en.wikipedia.org/wiki/Beaufort_scale
21. http://www.klmicrowave.com
22. http://www.mitidelmare.it
23. http://www.navigazionelaghi.it/
24. http://www.skymasts.com/home.aspx
25. IEC International Standard for AIS 61993-2, Part 2, December 2001.
26. Jackson, M.C., "The geometry of bistatic radar systems" IEE Proc., Vol.133, Part F., No.7, pp: 604-612, December 1986.
27. Long M. W., "Radar Reflectivity of Land and Sea", Artech House Boston, 2001.
28. Mahafza B., Elsherbeni A.: "MATLAB Simulations for Radar Systems Design", Chapman&Hall/CRC CRC Press LLC, 2004
29. Menelle M., G. Auffray, F. Jangal, "Full Digital High Frequency Surface Wave Radar: French Trials in the Biscay Bay", Radar, 2008, Adelaide, SA, pp.224-229
30. Nathanson F., J. P. Reilly, M. N. Cohen, "Radar design principles: signal processing and the environment", SciTech Publishing; 2 edition (January 1, 1999)
31. Rasmusson, Johan R.; Blom, Martin; Flood, Björn; Frölind, Per-Olov; Gustavsson, Anders; Jonsson, Tommy; Larsson, Björn; Stenström, Gunnar; Ulander, Lars M. H., "Bistatic VHF and UHF SAR for urban environments", Radar Sensor Technology XI. Edited by Kurtz, James L.; Tan, Robert J.. Proceedings of the SPIE, Volume 6547, pp. 654705 (2007).
32. Recommendation ITU-R M 1371 – 'Technical characteristics for a universal shipborne automatic identification system using time division multiplex access in the VHF maritime mobile band'.
33. Skolnik M., "Introduction to radar systems", Mcgraw-Hill, edition 1980
34. Skolnik, M. I. Radar Handbook. 2nd ed. Boston, Mass: McGraw-Hill, 1990.
35. Trizna D., Xu L., „Microwave and HF Multi-Frequency Radars for Dual-Use Coastal Remote Sensing Applications", OCEANS, 2005. Proceedings of MTS/IEEE, 2005, Vol.1, pp.532-537
36. Trizna, D.B.; "A bistatic HF radar for current mapping and robust ship tracking", OCEANS 2008, Sept 2008, pp.1-6
37. Ulander L.M.H., A. Barmettler B. Flood P.-O. Frölind, A. Gustavsson, T. Jonsson, E. Meier, J. Rasmusson, G. Stenström, "Signal-to-clutter ratio enhancement in bistatic very high frequency (VHF)-band SAR images of truck vehicles in forested and urban terrain", IET Radar, Sonar and Navigation, 2009
38. Vespe, M., Sciotti, M., Greidanus, H., Fortuny, J. "Potential of Passive-AIS Technology", IET Electronics Letters, Volume 46, Issue 20, pp: 1397–1399
39. W.A. Al-Ashwal, C.J. Baker, A. Balleri, H.D. Griffiths, R. Harmanny, M. Inggs, W.J. Miceli, M. Ritchie, J.S. Sandenbergh, A. Stove, R.J.A. Tough, K.D. Ward, S. Watts and K. Woodbridge "Statistical analysis of simultaneous monostatic and bistatic sea clutter at low grazing angles", Electronics Letters DOI 2011, vol.47, pp.621-622,
40. Willis N., Bistatic Radar, 2nd ed., Technology Service Corp., Silver Spring, MD, 1995, corrected and reprinted by SciTech Publishing, Inc., Raleigh, NC, 2005
41. Willis, N.J., Griffiths, H.D., 'Advances in Bistatic Radar', SciTech Publishing, 2007.

A P P E N D I X E S

Appendix 1: List of Abbreviations:

AIS – Automatic identification system
BT – Bandwidth Product
FM – Frequency Modulation
GCC – Generalized Cross Correlation
GMSK - Gaussian Minimum Shift Keying
GNSS – Global navigation Satellite System
HF – High Frequencies
IMO - International Maritime Organization
ITU – International Telecommunication Union
LNA – low noise amplifier
LPF – Low Pass Filter
MIMO – Multiple Input Multiple Output
MLE - Maximum Likelihood Estimation
P-AIS – Passive Automatic Identification System
PCL – passive coherent location
PNA - Program Network Analyzer
RCS – Radar Cross Section
RCSeff – Effective Radar Cross Section
SCR - Signal-to-Clutter-Ratio
SFLFM - Stepped Frequency Linear Frequency Modulation
SIR – Signal to Interference
SNR – Signal-to-Noise-Ratio
TDMA – Time Division Multiple Access
TDOA – Time Difference of Arrival
VCO – Voltage Controlled Oscillator
VHF – Very High Frequency

Appendix 2: Pictures from the in-situ experiments:

Figure A2.1: The bistatic detection experiment

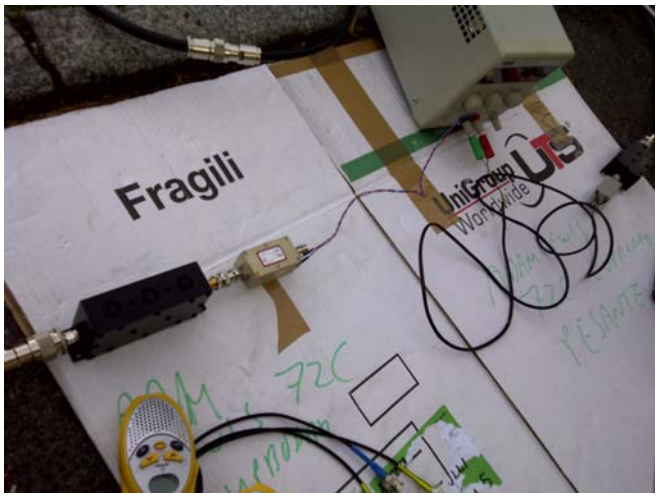

Figure A2.2: The bistatic system in process of assembly

Figure A2.3: The process of target RCS measurement

Appendix 3: Antenna patterns used in the experiments:

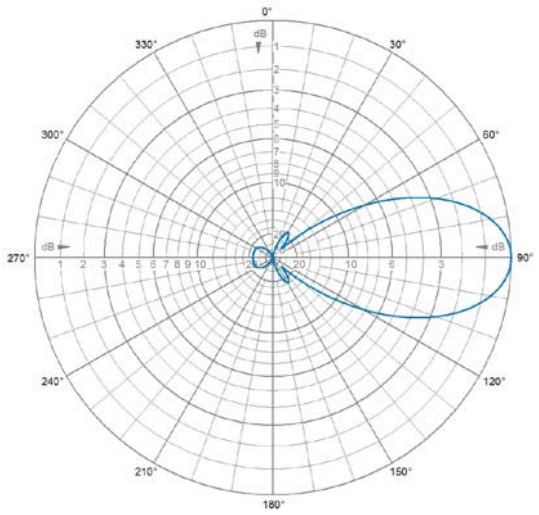

Figure A3.1: The antenna E- pattern used for the RCS detection experiment [24]

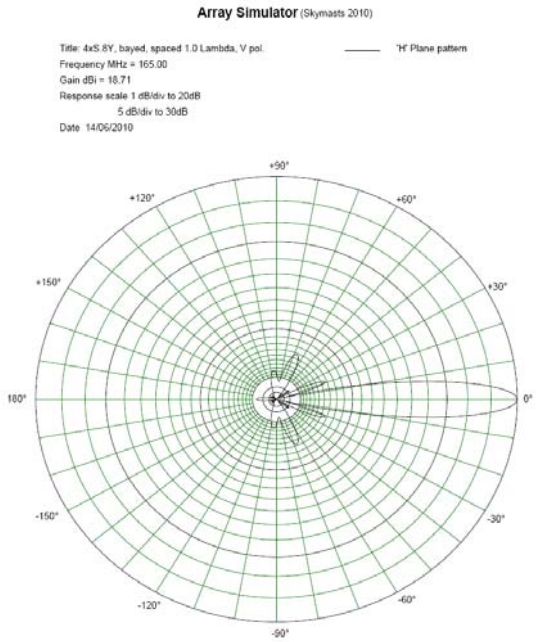

Figure A3.2: The antenna E- pattern of four elements receiving array [24]

Appendix 4: Target types description:

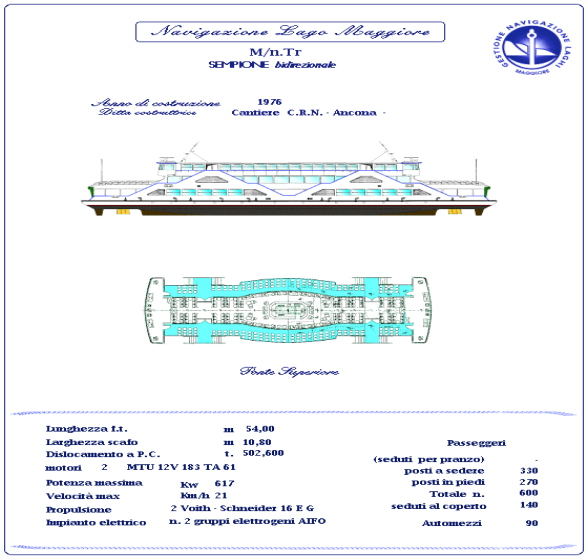

Figure A4.1: Type 1 - target description [23]

Figure A4.2: Type 2 - target description[22]

Figure A4.3: Type 3 - small wooden boat target description [22]

Appendix 5: Dynamically extract RCS procedure, used by us:

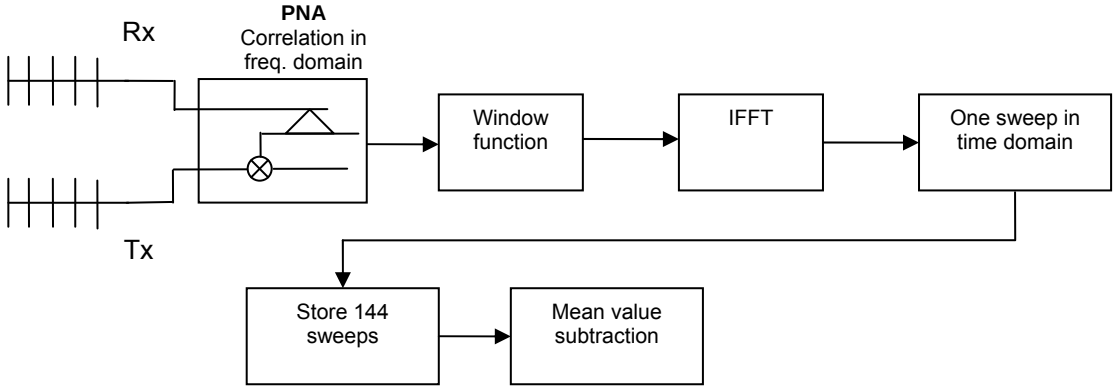

Figure A5.1: PNA as radar

The start frequency is: 146 MHz, stop frequency: 176MHz; 1601 frequency points, the frequency band is 30 MHz, the power of transitions is between 15 and 20dBm. Next diagram describes the signal processing algorithm in details. The used antennas pattern is shown on appendix 3. It is well known that the PNA is able to measure the S-parameter S21 – the forward voltage gain [1,2], which in our case, taking into consideration the power of the signal in the radar equation is $\frac{\Pr}{Pt} = S21^2$. Thus, the derivation for σ_{eff} of the effective RCS is estimated according to the simple radar equation is:

$$R_{\max} = \sqrt[4]{\frac{PtGtGr\lambda^2\sigma_{eff}}{\Pr(4\pi)^3}} \Rightarrow \sigma_{eff} = \frac{R_{\max}^4 \Pr(4\pi)^3}{PtGtGr\lambda^2}, \quad \frac{\Pr}{Pt} = S21^2,\ \sigma_{eff,dBsm} = 10\lg(\sigma_{eff}) \qquad (a5.1)$$

Procedure for dynamically RCS extraction:

1. Use the mean value range profile.

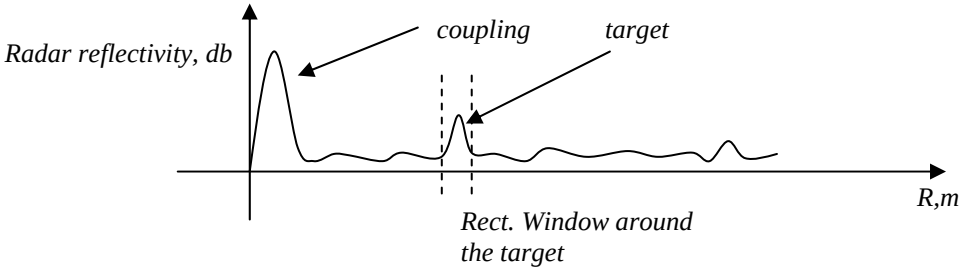

Figure A5.2: Procedure of dynamically RCS extraction

2. Separation the target with rectangular window and zeropad adding.

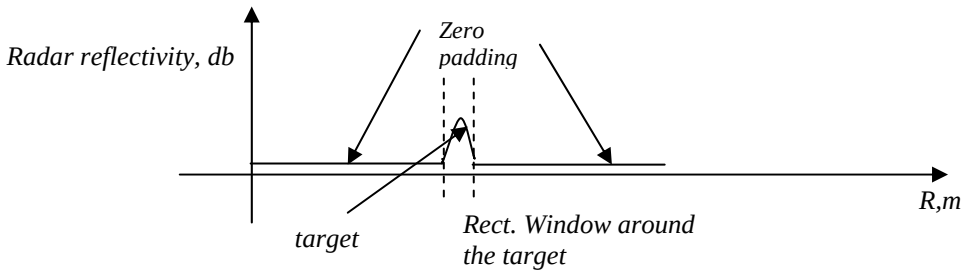

Figure A5.3: Procedure of dynamically RCS extraction

3. Transformation into the frequency domain.
4. De-windowing
5. Estimation the absolute value of the obtained S21
6. Estimation the mean value of the obtained S21
7. Substitution in eq.*a5.1*

European Commission
EUR 25169 EN – Joint Research Centre – Institute for Institute for the Protection and Security of the Citizen

Title: Passive Automatic Identification System for Maritime Surveillance

Authors: Vladimir Kyovtorov, Michele Vespe, Joaquim Fortuny-Guasch, Dario Tarchi, Raimondo Giuliani, Joan Broussolle

Luxembourg: Publications Office of the European Union

2012 – 40 pp. – 21.0 x 29.7 cm

EUR – Scientific and Technical Research series – ISSN 1831-9424

ISBN 978-92-79-22730-1

doi:10.2788/62028

Abstract

This work describes the main achievements in the Passive AIS (P-AIS) project stage. The extensive literature research in the second chapter concludes performing additional in-situ experiments to estimate reliable target RCS and clutter reflectivity values at the AIS frequency range. The typical effective RCS distribution for ferry, yacht and small wooden boat is experimentally drawn; it reaches up to 26dBsm for the ferry. A clutter model is created, taking into account the literature and the experimental study. The AIS signal waveform is analyzed and the potential range and Doppler resolution is defined. More specifically, the signal ambiguity function gives approximately 20km of range resolution and 40Hz Doppler resolution. A coverage prediction tool, based on the bistatic radar equation, including the aforementioned clutter model; bistatic geometry theory; the effective target RCS; the antenna pattern; the AIS air interface parameters is made. The tool estimates the possible P-AIS coverage area. The work concludes that: even in case of high sea state, the sea is considered as a smooth surface reflection for low grazing angle of observation in the VHF range; the equidistant SNR areas change from Cassini shape to single oval receiver centered; the AIS energy provides excellent target "visibility" if the clutter is not considered. Discussions for further clutter reduction and system sophistication are arisen.

LB-NA-25169-EN-N

As the Commission's in-house science service, the Joint Research Centre's mission is to provide EU policies with independent, evidence-based scientific and technical support throughout the whole policy cycle.

Working in close cooperation with policy Directorates-General, the JRC addresses key societal challenges while stimulating innovation through developing new standards, methods and tools, and sharing and transferring its know-how to the Member States and international community.

Key policy areas include: environment and climate change; energy and transport; agriculture and food security; health and consumer protection; information society and digital agenda; safety and security including nuclear; all supported through a cross-cutting and multi-disciplinary approach.

Publications Office

ISBN 978-92-79-22730-1

9 789279 227301